Biomedicine & Pharmacotherapy 194 (2026) 118887

Contents lists available at ScienceDirect

Biomedicine & Pharmacotherapy

journal homepage: www.elsevier.com/locate/biopha

Chemokine CCL5 overexpression combined with radiotherapy modulates Th1-mediated immune response and leads to significant tumor growth delay in mouse tumor models

Tim Bozic [a], Iva Santek [a,b], Ziva Pisljar [a], Simona Kranjc Brezar [a,b], Gregor Sersa [a,c], Bostjan Markelc [a,d,*], Maja Cemazar [a,e,*]

[a] Department of Experimental Oncology, Institute of Oncology Ljubljana, Zaloska cesta 2, Ljubljana, Slovenia
[b] Faculty of Medicine, University of Ljubljana, Vrazov trg 2, Ljubljana SI-1000, Slovenia
[c] Faculty of Health Sciences, University of Ljubljana, Zdravstvena pot 5, Ljubljana SI-1000, Slovenia
[d] Biotechnical Faculty, University of Ljubljana, Jamnikarjeva ulica 101, Ljubljana SI-1000, Slovenia
[e] Faculty of Health Sciences, University of Primorska, Polje 42, Izola SI-6310, Slovenia

ARTICLE INFO

Keywords:
Chemokines
CCL5
Gene therapy
Gene electrotransfer
Radiotherapy
Mouse tumor models

ABSTRACT

This study investigated the antitumor efficacy of chemokine CCL5 gene therapy using gene electrotransfer (GET) in combination with radiotherapy (RT) in solid murine tumors CT26 and 4T1. In vitro, CT26 and 4T1 tumor cells transfected with plasmid DNA (pDNA) encoding CCL5 induced migration of RAW264.7 macrophages. In vivo, CCL5 overexpression achieved via GET of pDNA encoding CCL5 led to increased splenocyte infiltration in dorsal window chamber models. When combined with RT, GET of pDNA encoding CCL5 shifted the tumor cytokine profile toward a proinflammatory state, with elevated Ifn-γ, Cxcl9, Cxcl10, and Il-12α. Although CD8 + and CD4 + T cells were reduced post-treatment, due to radiation-induced cell death, the combination of GET of pDNA encoding CCL5 and RT significantly delayed tumor growth in both models. In 4T1 tumors, this delay was also significant compared to the equivalent treatment with GET of control pDNA. These findings support GET of pDNA encoding CCL5 combined with RT as a strategy to enhance immune-mediated tumor control.

1. Background

Chemokines are one of the central chemoattractants and migratory stimulators of both immune and non-immune cells [1,2]. They orchestrate leukocyte trafficking under both physiological and pathological conditions, yet their precise role in the inflammatory environment of tumor development remains incompletely understood [3]. Based on their expression and function, chemokines are broadly categorized as homeostatic or inflammatory. Homeostatic chemokines regulate the normal trafficking of immune cells within secondary lymphoid organs and tissues [4]. Inducible chemokines are upregulated at sites of inflammation and recruit activated effector leukocytes to tissues in response to immunological stimuli. Given their unique ability to attract innate and adaptive effector immune cells, chemokine overexpression in solid tumors could potentially lead to increased infiltration of effector immune cells and thereby contribute to the development of new immunotherapy strategies in the field of oncology. While recent advancements in immunotherapies, targeting immune check points (ICs) offer promising outcomes in tumor control, a great fraction of patients remains unresponsive to immune checkpoint inhibitor (ICI) therapies [5]. Specifically, in patients, tumor immune status, which among other properties represents tumor's immune cell landscape, is often deprived of effector CD8 + and helper CD4 + T cells, crucial for effective antitumor immune response, which could be facilitated through chemokine mediation [6]. Within the broad family of chemokines, proinflammatory chemokine (C-C motif) ligand 5 (CCL5) or RANTES (regulated upon activation, normal T cell expressed and secreted) was associated with increased immune cell infiltration into various tumors [3,7].

Independent studies of cell migration showed that CCL5 displays affinity to chemokine receptors CCR1, CCR3 and CCR5, which are widely represented on the surface of CD4 + and CD8 + T lymphocytes, natural killer (NK) cells, dendritic cells (DCs) as well as tumor-associated macrophages (TAMs) [8,9]. Preclinical studies on spheroids and

* Corresponding authors at: Department of Experimental Oncology, Institute of Oncology Ljubljana, Zaloska cesta 2, Ljubljana, Slovenia.
E-mail addresses: bmarkelc@onko-i.si (B. Markelc), mcemazar@onko-i.si (M. Cemazar).

https://doi.org/10.1016/j.biopha.2025.118887
Received 2 July 2025; Received in revised form 27 November 2025; Accepted 3 December 2025
Available online 6 January 2026

transgenic mouse models associated *Ccl5* overexpression in tumors with cytotoxic T lymphocyte infiltration and significant tumor growth delay in ovarian cancer [3]. Besides guiding T lymphocytes to tumor location, CCL5 also participates in CD4 + helper-dependent CD8 + T lymphocyte activation [10]. Notably, the levels of CCL5 produced by NK cells originating from tumor microenvironment (TME) also correlate with DC accumulation, which in turn drive the antitumor immunity through antigen presentation and effector T lymphocyte activation [11,12]. Meta-analysis of a large clinical data showed that *CCL5* and *CXCL9* co-expression is needed for the CD8 + T lymphocyte infiltration and increased overall survival in multiple human tumors [3]. Moreover, increased *CCL5* expression in triple negative breast cancer patients was associated with the recruitment of effector immune cell populations [13]. Elevated CCL5 expression has been reported in multiple tumor types, including breast, brain, head and neck, liver, pancreatic, colorectal, prostate, and oral cancers [14–21]. In early breast cancer patients, increased CCL5 serum levels correlated with prolonged disease-free survival [22]. More importantly, several studies demonstrated the benefits of using CCL5 as an adjuvant for enhancing anti-tumor immunity [23].

Expanding on the immunomodulatory role of CCL5, several independent gene therapy studies have explored its use through various delivery systems. Dangaj et al. [3] demonstrated in a preclinical study using the ID8 syngeneic mouse ovarian cancer model that sustained expression of CCL5 led to a significant delay in tumor growth and prolonged survival, primarily through enhanced recruitment of $CD8^+$ T cells. A detailed analysis of the CCL5 signaling cascade further revealed the involvement of other IFN-γ–inducible T helper 1 (Th1)–type chemokines, such as CXCL9 and CXCL10, which were shown to be epigenetically silenced in tumor cells but otherwise play key roles in preventing immune escape and promoting $CD8^+$ T-cell infiltration in ovarian and other cancer types [24]. Moreover, CCL5 has been assessed in combination with PD-1/PD-L1 inhibitor therapy and provided optimistic results [25]. However, in patients lacking immune checkpoints combining chemokine overexpression with ICI therapies is not applicable [26]. In these cases, radiotherapy (RT), used in over half of all cancer patients, offers an effective alternative. RT not only induces direct tumor cell death but also promotes antitumor immunity by enhancing antigen presentation, increasing lymphocyte infiltration, and modulating tumor vasculature [27,28]. Additionally, irradiation (IR) can activate DNA sensors and the cGAS-STING signaling pathway, triggering the secretion of inflammatory cytokines and other inflammatory factors [29]. A form of cell death known as immunogenic cell death (ICD), which can be triggered by IR, is responsible for many of these indirect immunological effects, ultimately transforming a non-immunogenic TME into an immunogenic one [30].

In our previous study we determined the impact of CCL5 on the TME using murine breast (4T1, E0771) and colon (CT26, MC38) cancer models [31]. We employed pDNA encoding CCL5 chemokine, delivered via lipofection in vitro and gene electrotransfer (GET) in vivo, to achieve their overexpression within tumor cells. Both in vitro lipofection and in vivo GET of pDNA encoding CCL5 demonstrated robust transgene expression and upregulation of Th1-type proinflammatory cytokines *Il-6*, *Ifn-γ*, *Cxcl9*, *Cxcl10*, *Il-12α* across all investigated cancer cell lines and tumor models. However, in vivo GET of pDNA encoding CCL5 yielded an unsignificant anti-tumor effects in CT26 and 4T1 tumor models, suggesting that GET of pDNA encoding CCL5 monotherapy is insufficient for an enhanced anti-tumor effectiveness.

Based on these results, our aim was to investigate the GET of pDNA encoding CCL5 in combination with RT in the murine colon cancer model CT26 and the breast cancer model 4T1. Although RT has the potential to activate immune cells, a significant challenge lies in the absence or insufficient presence of immune cells within the TME [32]. By combining GET-mediated delivery pDNA encoding CCL5 with RT, this approach aimed to recruit immune cells to tumors, thereby enabling their activation through irradiation-induced immunological effects.

2. Methods

2.1. Study design

This study investigates the role of CCL5 GET combined with RT in immune cell recruitment and tumor response in murine tumor models CT26 and 4T1. In vitro, RAW264.7 macrophage migration was observed toward CCL5-transfected CT26 and 4T1 tumor cells to assess the chemotactic potential of CCL5. In vivo, splenocyte infiltration into tumors was determined using dorsal window chamber models (DWCs) after GET of pDNA encoding CCL5. To evaluate the therapeutic effects of GET of pDNA encoding CCL5 combined with IR, tumors were treated according to the scheme in Fig. S10. GET was always performed in combination with IR, while IR was applied either alone or in combination with GET. In the case of combined treatments with double GET and fractionated IR, the second GET was performed on day 4 after the initial treatment. For immunofluorescence and gene expression analysis, irradiated and control tumors were collected at the same time point, on day 3 after the last IR dose.

2.2. Plasmids

The plasmids pUNO1-mcs (control, non-coding pDNA Ctrl) and pUNO1-mCCL5 (pDNA encoding CCL5) were purchased from InvivoGen (Toulouse, France). All plasmids were amplified in a competent *Escherichia coli* (JM109; Thermo Fisher Scientific, MA, US) and purified using the EndoFree Plasmid Mega (Qiagen, Hilden, Germany) kit according to manufacturer's instructions. The concentration of isolated plasmids was measured with Qubit DNA Broad Range kit (Thermo Fisher Scientific) by fluorometric quantification using Qubit 4 Fluorometer (Thermo Fisher Scientific). Quality and integrity of isolated plasmids were confirmed by measuring the 260/280 nm absorbance ratio using an Epoch Microplate Spectrophotometer (BioTek Instruments GmbH, Bad Friedrichshall, Germany) and by agarose gel electrophoresis. For the experiments, all plasmids were diluted in physiological saline to a final concentration of 1 μg/μL or 2 μg/μL.

2.3. Cell cultures

Murine colon cancer cell line CT26 and breast cancer cell line 4T1, macrophages RAW264.7 and human embryonic kidney 293 T cell line were originally purchased from ATCC (VA, US). Cells were cultured in a humidified incubator at 37 °C, in an atmosphere of 5 % CO_2 and 95 % relative humidity. To generate fluorescently labeled tumor cell lines, CT26 and 4T1 cells with stable expression of green fluorescent protein (GFP) (CT26-GFP and 4T1-GFP) were established by lentiviral transduction using the pLenti-PGK-GFP-Puro plasmid (Addgene, MA, US). Lentiviruses were produced in 293 T packaging cells (ATCC) using the plasmids pMD2.G, pMDLg/pRRE, and pRSV-Rev (Addgene) introduced via lipofection. GFP-positive CT26 and 4T1 monoclonal colonies were selected using puromycin (Sigma-Aldrich, Darmstadt, Germany).

CT26, CT26-GFP, 4T1, 4T1-GFP and RAW264.7 cells were cultured in Advanced RPMI 1640 (Gibco, Thermo Fisher Scientific, VA, US), while 293 T cells were cultured in Advanced DMEM (Gibco, Thermo Fisher Scientific, VA, US). Media were supplemented with 5 % FBS (Gibco), GlutaMAX (100 ×, Gibco), and Penicillin-Streptomycin (100 ×, Sigma-Aldrich). The cells were routinely tested for mycoplasma infection by MycoAlertTM PLUS Mycoplasma Detection Kit (Lonza, Basel, Switzerland) and were mycoplasma free. Cells were subcultured twice weekly using 0.025 % trypsin with 0.75 mM EDTA, except RAW264.7 macrophages, which were detached using a cell scraper (TPP, Trasadingen, Switzerland). For experiments, low-passage (<15) cells in the exponential growth phase were used and counted with a CytoSMART cell counter (CytoSMART Technologies, Eindhoven, Netherlands).

2.4. Lipofection

CT26 and 4T1 tumor cells were transfected with plasmid DNA (pDNA) encoding CCL5 or with non-coding control plasmid (pDNA Ctrl) using Lipofectamine 2000 (1 mg/μL solution; Thermo Fisher Scientific) and Opti-MEM medium (Gibco) according to the manufacturer's instructions. Transfections were performed in T75 flasks at 80 % confluency, 48 h prior to the chemotaxis experiment. Non-transfected CT26 and 4T1 cells served as additional controls.

2.5. Chemotaxis assays

The chemotactic properties of chemokine CCL5 were determined in vitro using Culture-Inserts 4 Wells (Ibidi, WI, US). Twenty-four hours before the experiment, RAW264.7 macrophages were labeled with the fluorescent dye CellTrace™ CFSE (Invitrogen) according to the manufacturer's protocol. 24 h before the experiment RAW264.7 cells were labeled with the fluorescent dye CellTrace™ CFSE Dye (Invitrogen) according to the manufacturer's instructions. After staining the silicon inserts with four wells (Culture-Inserts 4 Well, Ibidi) were first attached to the bottom of a 24-well plate using sterile tweezers. In two parallel wells of the insert, 5×10^4 transfected CT26 or 4T1 cells were seeded, and in the opposite two parallel wells, 1×10^5 RAW264.7 macrophages were seeded, each in 100 μL of Advanced phenol-free RPMI-1640 medium (Gibco™, Thermo Fisher Scientific) to reduce imaging background. After 24 h, the silicon inserts were removed and macrophage migration was monitored for 20 h in a controlled environment (37°C and 5 % CO_2 atmosphere) using the Cytation 1 and Gen5 software (BioTek Instruments), with fluorescent images captured at 30-minute intervals. For imaging, a 4x magnification objective (4x, 0.13 NA Olympus Plan Fluorite) was used, along with an LED light source and a filter cube that transmitted excitation light at 445–495 nm and emission light at 505–555 nm. Images were acquired using a CCD camera with 16-bit grayscale depth.

2.6. Mice

Immunocompetent 6–8-weeks-old Balb/c (BALB/cAnNCrl) female mice were obtained from Charles River Laboratories (MA, US). Mice weighted between 18 and 20 g at the beginning of the experiments and were kept in a specific pathogen-free environment with 12-hour light-dark cycle at 20–24 °C with 55 % ± 10 % relative humidity and food and water provided ad libitum. The experiments were approved by the Ministry of Agriculture, Forestry and Food of the Republic of Slovenia (permits U34401–1/2015/43, U34401–1/2020/8 and U34401–3/2022/17) and were in compliance with the European Directive on animal experiments (2010/63/EU). Mice were housed in individually ventilated cages (IVC rack system; Animal Care Systems Inc., Revere Parkway, USA) with up to six animals per cage and provided with environmental enrichment (Bio-Serv, VWR, PA, US). During all procedures, mice were anesthetized with 2 % (v/v) isoflurane (Isoflurane; Piramal Healthcare UK Limited, London, UK) unless stated otherwise. All experiments adhered to the principles of the 3Rs and followed the ARRIVE [33], PREPARE [34], and OBSERVE [35] guidelines.

2.7. Dorsal window chamber models

Surgical implantation of DWCs was carried out according to a published protocol [36]. Briefly, titanium frames were surgically implanted on the backs of mice under sterile conditions and systemic anesthesia (1 mg/mL ketamine (Narketan, Vetoquinol AG), 5 mg/mL xylazine (Chanazine, Chanelle Pharmaceuticals), and 0.4 mg/mL acepromazine (Promace, Fort Dodge Animal Health), with pain minimized by administering ketoprofen (3.5 mg/kg, Ketonal, Lek d.d.). After 24 h, tumors were established by subcutaneous injection of 3×10^5 CT26-GFP or 4T1-GFP cells in 5 μL of 0.9 % NaCl saline. Transfection of tumors with pDNA encoding CCL5 and control pDNA (pDNA Ctrl) using GET was performed when tumors reached the volume of 25 mm^3 (calculated using formula: V = a × bˆ2 × π/6) as described under Gene electrotransfer section. After 48 h, mice were intravenously injected via the tail vein with a suspension of 5×10^6 fluorescently labeled naïve splenocytes (CM-DiI Dye, Thermo Fisher Scientific) in 100 μL of saline. Naïve splenocytes were isolated on the day of the injection from spleen of healthy donor mice. Three-dimensional (3D) immunofluorescence images of tumors in dorsal windows were captured using a Zeiss LSM 800 confocal microscope (Carl Zeiss, Oberkochen, Germany) equipped with a 20x magnification objective (NA 0.8). Laser light at specific excitation wavelengths (GFP, Alexa Fluor 488: 488 nm; Cy3: 561 nm) was used during imaging, which was performed in complete darkness. Fluorescent emission was detected using a gallium arsenide phosphide (GaAsP) detector with a variable beam splitter and wavelength-specific filters (Alexa Fluor 488: 488–545 nm; Cy3: 565–620 nm). The imaging depth, defined by the distance between the extreme focal planes, was set to 100 μm, with a 5 μm step between each image in the Z-direction.

2.8. Tumor induction and measurement

One day prior to the experiment, the backs of the mice were shaved and randomly divided into experimental groups. Tumor induction in mice receiving combined therapies of GET and IR was carried out by subcutaneous injection of 3×10^5 CT26 or 4T1 cells in 100 μL of 0.9 % NaCl saline. Tumor volumes were measured every other day using a caliper (Model CD-15DAX, Mitutoyo, Kanagawa, Japan). The measurements were recorded in In-Life&Tumor software (Labcat, Innovative Programming Associates, Inc., NJ, US) using on the ellipsoid volume formula ((a × b × c × π/6), where a, b, and c represent perpendicular tumor diameters). After approximately 7–10 days, tumors reached a volume of 50 mm^3 , at which point therapy was initiated, as outlined in the study design (Fig. S10). Animals were sacrificed when tumors reached the maximal volume of 500 mm^3 or if tumors showed signs of ulceration. Tumor volume of 500 mm^3 was counted as a humane end point for the construction of the Kaplan-Meier curves. Tumor growth delay was calculated as the difference in time when tumors doubled in volume between the control group and the treated group. Additionally, the weight of the mice and their behavior was assessed using the mouse grimace scale (MGS) [37]as an indicator of systemic toxicity of the therapy.

2.9. Immune rechallenge experiment

To assess the development of long-term immune memory after therapy, tumor-free mice that achieved complete response (CR) were subjected to an immune re-challenge. Fourteen days after complete tumor regression, mice were subcutaneously injected with 3×10^5 CT26 or 4T1 cells (corresponding to their original tumor model) in the right flank, in 100 μL of 0.9 % NaCl saline. No additional treatment was administered. Tumor growth in re-challenged mice was monitored for 90 days. Mice that remained tumor-free throughout the observation period were considered to have developed protective immune memory.

2.10. Gene electrotransfer

At the start of the therapy intratumoral injection of either 25 μg (25 μL of 1 μg/μL pDNA) or 50 μg (25 μL of 2 μg/μL pDNA) of the pDNA Ctrl or pDNA encoding CCL5, was injected using a 29 G insulin syringe. Different amounts of pDNA were used to evaluate dose-dependent effects and to minimize confounding effects caused by the plasmid itself. Lowering the pDNA dose to 25 μg aimed to limit the activation of DNA sensors, which can trigger innate immune responses independent of the therapeutic chemokine. This strategy helped to better assess the specific contribution of the pDNA encoded CCL5 to the observed therapeutic outcomes.

After 5 min GET was performed by the application of electric pulses routinely used in clinics for electrochemotherapy (ECT pulses: 8 pulses, 1300 V/cm, 100 μs, 1 Hz). This protocol was chosen because short, high voltage electric pulses are already successfully used for gene therapy [38,39]. The pulses were generated by ELECTRO Cell B10 electric pulse generator (Leroy biotech, France). For combined treatments, 6 mm parallel stainless-steel plate electrodes were used. During GET a conductive gel (Gel G006 ECO, FIAB, Vicchio, Italy) was used at the contact of the electrodes and the skin overlaying tumors to ensure good conductivity. The electrodes were positioned around the tumor, ensuring the tumor was located between them. Four electric pulses were delivered in one orientation, followed by four additional pulses delivered perpendicular to the initial orientation [40].

For DWCs, due to the smaller tumor size, a lower dose of 10 μg (5 μL of 2 μg/μL plasmid DNA) was intratumorally injected 5 min before GET, which was performed using 4 mm parallel stainless-steel plate electrodes.

2.11. Irradiation

Tumors were irradiated with either a single dose of 10 Gy or a fractionated dose of 3 × 5 Gy using the CP225 X-ray system (Gulmay Medical Ltd., Surrey, UK) with 0.55 mm Cu and 1.8 mm Al filtering. The dose was delivered exclusively to the tumor, with the mice restrained in lead shielding to protect non-tumor tissues. During irradiation, mice were not under anesthesia. The IR dose rate was 1.92 Gy/min. Both regimens delivered a biologically effective dose (BED) of approximately 22 Gy, calculated using the BED equation with an α/β ratio of 10, suitable for tumors and tissues with early or acute responses to IR [41].

2.12. Tumor collection

Mice were euthanized and tumors were surgically removed. Immediately after, one-half of the collected tumor was weighted and frozen in liquid nitrogen. Frozen tumor samples were crushed using a pestle and then stored at −80℃ before RNA extraction. The other half of the tumor was first fixed in 4 % paraformaldehyde (PFA; Alfa Aesar) overnight, then incubated in 30 % sucrose for 24 h, embedded in Optimal cutting temperature compound (OCT compound) and snap-frozen in liquid nitrogen before RNA extraction.

2.13. Gene expression analysis

Frozen tumor samples were crushed using a pestle and then stored at −80℃ before RNA extraction. Total RNA was extracted from treated tumors using the Total RNA Kit, peqGOLD (VWR), following the manufacturer's protocol. Cell lysis was performed with TRI Reagent (Thermo Fisher Scientific). RNA concentration was measured using the Qubit DNA Broad Range Kit (Thermo Fisher Scientific) on a Qubit 4 Fluorometer (Thermo Fisher Scientific).

First-strand (5′ to 3′ direction) cDNA was generated from 2 μg of template RNA using a Thermocycler Primus 25 (Peqlab, UK) and SuperScript VILO cDNA Synthesis Kit (Thermo Fisher Scientific) in a 20 μL reaction mix, according to the manufacturer's instructions. Priming was performed at 25℃ for 10 min and reverse transcription for 60 min at 42℃. The cDNA was then stored at −20℃ for subsequent analysis. Quantitative Polymerase Chain Reaction was performed with LightCycler 480 (Roche, Basel, Switzerland). The samples were prepared using TaqMan Gene Expression Assays of predesigned chemokine and cytokine specific primers (IDT, IA, US) (Table S1). Briefly, the thermocycling protocol consisted of initial denaturation at 95 °C for 2 min, followed by 40 cycles of 95 °C for 15 s and 60 °C for 60 s. All samples were run in duplicates and the products were analyzed on LightCycler 480 (Roche). Relative quantification was performed by comparison to the housekeeping genes RNA polymerase II subunit A (Polr2a). No-template controls were included for each primer set on every plate.

2.14. Immunofluorescence

Fourteen-micrometer thick frozen tissue sections were prepared using Leica CM1850 cryostat (Leica, Wetzlar, Germany) and stained with primary (Table S2) and secondary (Table S3) antibodies. Staining was performed by first drying the sections for 10 min at 37°C and then washing them twice for 5 min in 1x PBS. Antigen retrieval was then performed by putting the slides in a hot citrate buffer (approx. 95°C) which was cooled down on air, at 25°C for 30 min followed by a 30 min cooling in water. After the washing in PBS, the sections were blocked/permeabilized in blocking buffer (0.5 % Tween 20, 5 % donkey serum, 22.52 mg/mL glycine in PBS) for 30 min at 25°C in a humidified chamber. Sections were then blocked again for 1 h in 5 % donkey serum and incubated overnight at 4 °C with primary antibodies diluted in blocking buffer (2 % donkey serum, 22.52 mg/mL glycine in PBS) in a humidified chamber. After washing thrice in PBS, sections were incubated with secondary in blocking buffer (2 % donkey serum, 22.52 mg/mL glycine in PBS) for 1 h at 25°C in a humidified chamber and then washed thrice in PBS. Nuclei were counter-stained with Hoechst 33342 solution (3 μg/mL) in PBS for 10 min in the dark. After another two washes in PBS, slides were mounted with ProLong™ Glass Antifade Mountant (Thermo Fisher Scientific). Three tumor samples per group were imaged using a Zeiss LSM 800 confocal microscope (Carl Zeiss) equipped with a 20 × /0.8 NA objective. Hoechst 33342, Alexa Fluor 488, Cy3, and Alexa Fluor 647 were excited with 405, 488, 561, and 640 nm lasers, respectively. Emission signals were captured using a Gallium Arsenide Phosphide (GaAsP) detector and a variable dichroic filter with wavelength ranges of 410–545 nm (Hoechst 33342), 488–545 nm (Alexa Fluor 488), 565–620 nm (Cy3), and 645–700 nm (Alexa Fluor 647). The obtained images were visualized and analyzed with Imaris software (Oxford Instruments, Abingdon, UK). Cutoff thresholds for each channel were determined based on negative controls.

2.15. Statistical analysis

Statistical analysis and graph plotting were done using GraphPad Prism 10 (Dotmatics, CA, US). Normal distribution of the data was tested using D'Agostino-Pearson normality test. Statistical significance was evaluated using with One-way ANOVA with Dunnett's multiple comparisons *post hoc* test or *t*-test. The Log-Rank test was used to detect statistical differences in survival probabilities on Kaplan-Meier curves for each comparison and calculated the adjusted p-value using the Holm-Šídák method. Normalized tumor growth delay was calculated by adjusting individual tumor growth delay to average tumor growth delay of control.

Treatment responses were analyzed using the DRAP package [42] in R. Individual mouse responses were classified according to the Novartis Institutes for BioMedical Research PDX encyclopedia (NPDXE) response criteria as implemented in DRAP. NPDXE response was determined by comparing the tumor volume change at time t relative to baseline: % tumor volume change = ΔVolt = 100 % × ((Vt – Vinitial) / Vinitial). The BestResponse was defined as the minimum ΔVolt value for $t \geq 10$ days. For each time point t, the average ΔVolt from t = 0 to t was also calculated, and the BestAvgResponse was defined as the minimum of this average for $t \geq 10$ days. This metric captured the combination of speed, strength, and durability of response into a single value. The NPDXE response criteria were applied in the following order: complete response (CR), BestResponse < -95 % and BestAvgResponse < -40 %; partial response (PR), BestResponse < -50 % and BestAvgResponse < -20 %; stable disease (SD), BestResponse < 35 % and BestAvgResponse < 30 %; and progressive disease (PD), not otherwise categorized.

In addition to these standard criteria, we implemented a custom CR rule: any mouse whose tumor volume measured 0 mm^3 for five consecutive time points at the end of the observation period was classified as CR, regardless of its NPDXE classification. Conversely, if the

NPDXE criteria assigned a CR but the custom rule was not met, the response was downgraded to PR. This adjustment ensured that gradual complete regressions persisting over time were accurately captured and that isolated measurement artifacts did not inflate CR classification.

Throughout the manuscript the following symbols indicate statistical significance: *p < 0.05, **p < 0.01, ***p < 0.001, and ****p < 0.0001. The sample size (N) for each experiment is presented in the Fig. legends and represents the number of biological replicates.

3. Results

3.1. CCL5-transfected CT26 and 4T1 tumor cells induce migration of RAW264.7 macrophages in vitro

To validate the pDNA encoding CCL5 and its biological function we first sought to determine the chemotactic ability of CCL5 in vitro and in vivo. In vitro we determined macrophage RAW264.7 migration towards CT26 and 4T1 tumor cells transfected via lipofection with pDNA encoding CCL5 or non-coding pDNA (pDNA Ctrl). Macrophage migration toward transfected CT26 and 4T1 cells was observed 48 h after lipofection, with migration monitored for 20 h (Fig. 1, Movie S1). In assays with the CT26 cell line, the highest macrophage migration was observed toward tumor cells transfected with pDNA encoding CCL5, compared to the control and pDNA Ctrl. The difference in the number of migrating macrophages between groups increased over time. While the number of migrating macrophages toward CCL5-transfected CT26 cells gradually increased over time, migration toward untreated and CT26 cells transfected with pDNA Ctrl showed a steady but nonsignificant decrease over time (Fig. 1A). The increase in the number of migrating macrophages toward 4T1 cells transfected with individual pDNA was more linear compared to CT26 cells (Fig. 1B). The difference in migrating macrophage numbers between groups increased over time and, unlike in assays with CT26 cells, never reached a plateau. Among groups, CCL5 induced the highest macrophage migration in transfected 4T1 cells.

Supplementary material related to this article can be found online at doi:10.1016/j.biopha.2025.118887.

At the 10-hour time point, macrophage migration toward CCL5-expressing CT26 cells was about 1.4 times higher than toward cells transfected with pDNA Ctrl (Fig. 1Ci). Similarly, in the 4T1 assays, the number of migrating macrophages toward CCL5-transfected cells was significantly higher compared to both the pDNA Ctrl-transfected cells and untreated control (Fig. 1Di). At the 20-hour time point, macrophage migration toward CT26 cells transfected with CCL5 was 2 times higher compared to pDNA Ctrl (Fig. 1Cii). In 4T1 cells, migration toward CCL5-transfected cells remained significantly higher than control, with a 1.4-fold increase compared to pDNA Ctrl (Fig. 1Dii). Although untreated tumor cells can induce notable chemotaxis of murine RAW264.7 macrophages, these results suggest that transfection with CCL5 significantly enhances their migration in both cell lines.

3.2. In vivo dorsal window chamber experiments show that GET of pDNA encoding CCL5 induces infiltration of naïve splenocytes only in 4T1 tumors

In the in vivo experiment, the DWCs were used to determine the extravasation of fluorescently labeled splenocytes, isolated from the spleens of healthy donor mice, into CT26-GFP and 4T1-GFP tumors 24 and 48 h after their injection into the tail vein. We determined the number of infiltrated splenocytes within the tumors (intratumoral) by modeling the tumor volume as well as those outside the tumors in the surrounding visible area (peritumoral) (Fig. S1). Differences in the infiltration of splenocytes between the control and treated groups were already apparent from the representative immunofluorescence images after intravenous injection (Fig. 2A and B). Compared to the control, the images of the treated groups showed increased infiltration of splenocytes within the tumors.

At 24 h, neither GET of pDNA encoding CCL5 nor pDNA Ctrl significantly increased splenocyte infiltration into CT26 tumors.

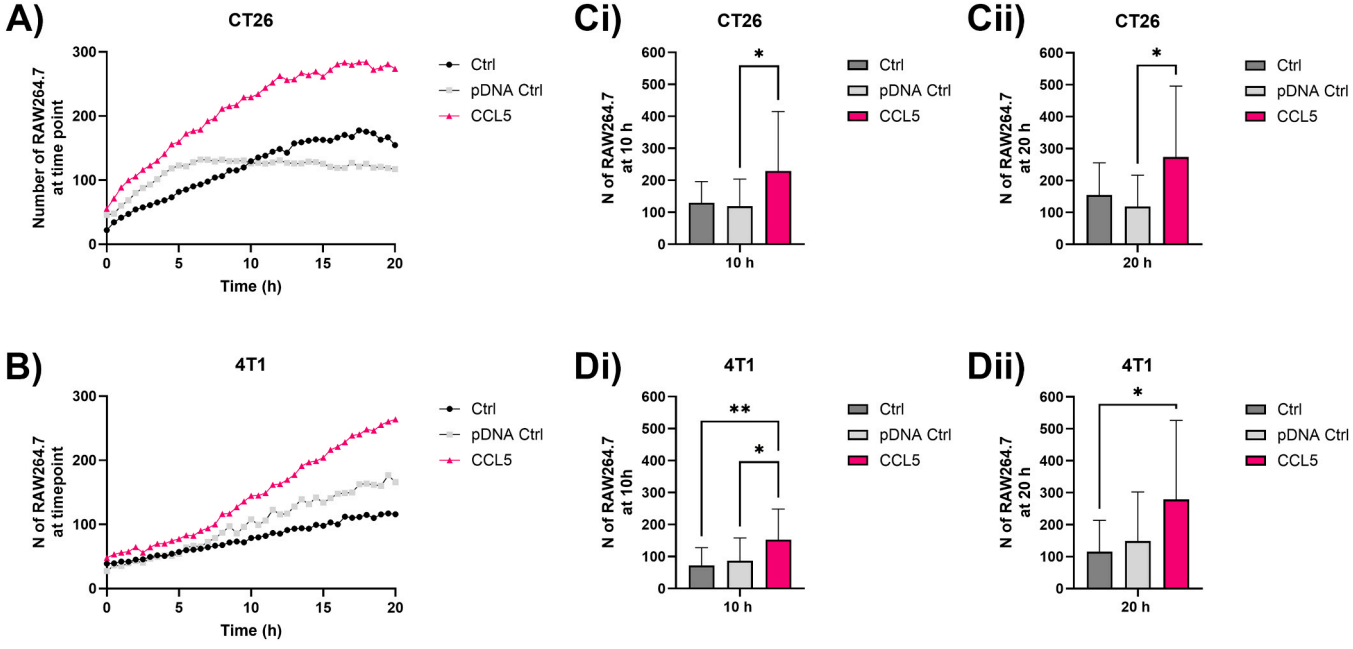

Fig. 1. Macrophage migration toward CCL5-overexpressing CT26 and 4T1 tumor cells. A, B) Graphs show the number of migrating murine RAW264.7 macrophages towards transfected CT26 and 4T1 tumor cells 48 h after lipofection with individual pDNA. Migration was monitored continuously for 20 h at 30-minute intervals, and data are presented as the arithmetic mean (AM). Graphs Ci) and Cii) show the number of migrating macrophages toward CT26 tumor cells, and Di) and Dii) toward 4T1 tumor cells, with Ci) and Di) corresponding to the 10-hour time point and Cii) and Dii) to the 20-hour time point. Data represent the arithmetic AM ± standard error of mean (SEM) of all replicates (N = 15). Statistical significance was determined by a *t*-test. A p-value of < 0.05 was considered to be statistically significant (*p < 0.05, **p < 0.01 vs control, non-treated tumor cells (Ctrl)). Ctrl: control group; pDNA Ctrl: Lipofection with pDNA Ctrl; CCL5: Lipofection with pDNA encoding CCL5.

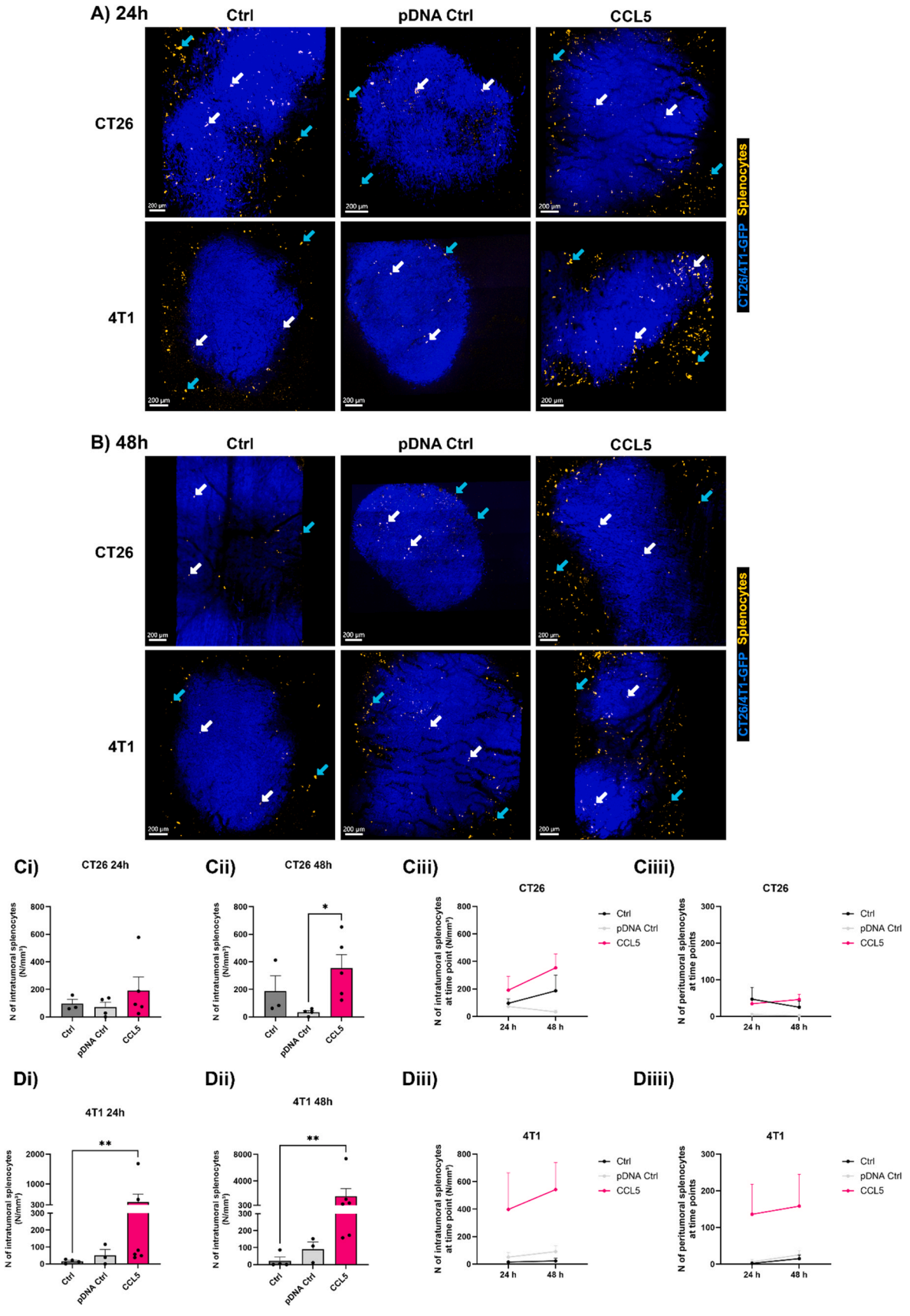

(caption on next page)

Fig. 2. Naïve splenocyte migration in the DWCs of CT26 and 4T1 tumors after GET of pDNA encoding CCL5. Individual representative images of the DWCs show splenocyte (yellow; Cy3) infiltration into CT26-GFP and 4T1-GFP tumors (blue; CT26/4T1-GFP) following GET of individual pDNA. Images were captured at A) 24 and B) 48 h after intravenous injection of splenocytes. White arrows indicate intratumoral splenocytes, while cyan arrows indicate peritumoral splenocytes. Yellow: splenocytes; blue: Hoechst33342. Scale bar: 200 μm. Quantification of splenocyte infiltration is shown in graphs Ci-Ciiii) and Di-Diiii). The number of intratumoral splenocytes in CT26-GFP tumors was determined at Ci) 24 and Cii) 48 h after injection. Graph Ciii) shows the number of peritumoral splenocytes in CT26-GFP tumors at both time points. Similarly, in 4T1-GFP tumors, Di) and Dii) show the number of intratumoral splenocytes at 24 and 48 h after injection, respectively, while graph Diii) shows the number of peritumoral splenocytes at both time points. The number of intratumoral splenocytes is normalized to the tumor volume (N/mm^3) within the visible field. All data represent the AM ± SEM of all replicates ($3 \leq N \leq 6$). Statistical significance was determined using a *t*-test. A p-value of < 0.05 was considered to be statistically significant (*$p < 0.05$, **$p < 0.01$ between groups). Ctrl: control group; pDNA Ctrl: GET of pDNA Ctrl; CCL5: GET of pDNA encoding CCL5. [43,44].

Specifically, GET of pDNA encoding CCL5 resulted in about 2 times higher number of intratumoral splenocytes compared to control (Fig. 2Ci). However, while these increases in splenocyte infiltration were observed, the differences between groups were not statistically significant due to the relatively high baseline number of infiltrated splenocytes in the untreated, control CT26 tumors. At 48 h the average number of intratumoral splenocytes in control and CCL5-treated tumors increased by approximately 49 %, compared to that of 24-hour time point (Fig. 2Cii). This increase was statistically significant in CCL5-treated tumors compared to GET of pDNA Ctrl, while the decrease in splenocyte numbers in the pDNA Ctrl group compared to control was not statistically significant (Fig. 2Cii and Ciii). In the 4T1 tumor model the basal number of infiltrated splenocytes in control group was lower compared to control CT26 tumors (Fig. 2Di). At 24 h GET of pDNA encoding CCL5 resulted in significant increase in the infiltration of splenocytes into 4T1 tumors compared to control. The number of intratumoral splenocytes after GET of pDNA Ctrl was similar to that observed in the control. In particular, the mean number of intratumoral splenocytes after GET of pDNA encoding CCL5 was about 26 times higher than in the control and 8 times higher compared to GET of pDNA Ctrl. At 48-hour time point, the number of intratumoral splenocytes further increased by almost 27 % after GET of pDNA encoding CCL5 (Figs. 2Dii and 2Diii).

In the surrounding visible area, the average number of peritumoral splenocytes was higher in 4T1 tumors compared to CT26 tumors, but remained comparable between corresponding groups at both time points (Fig. 2Ciiii and Diiii).

3.3. GET of pDNA encoding CCL5 combined with irradiation induces increased co-expression of proinflammatory cytokines associated with T cell infiltration

The expression of proinflammatory chemokines and cytokines in treated tumors was determined in the control group, after single-dose IR of 10 Gy or fractionated IR of 3 × 5 Gy and in therapies of GET of pDNA encoding CCL5 or pDNA Ctrl combined with IR (Fig. 3).

The selected cytokines, *Ifn-γ*, *Cxcl9*, *Cxcl10*, *Il-6*, and *Il-12α*, were analyzed because of their well-established roles in T-cell recruitment, Th1 activation, and antitumor immune responses [4]. CCL5 acts primarily through CCR5-mediated signaling, which can activate the JAK/STAT and NF-κB pathways, promoting the transcription of IFN-γ and IL-12 and establishing a positive feedback loop that amplifies Th1-type immune activation [4]. IFN-γ, in turn, induces the expression of CXCL9 and CXCL10, chemokines that recruit CXCR3$^+$ effector CD4$^+$ and CD8$^+$ T cells into tumors. These cytokines cooperate functionally: IL-12 enhances IFN-γ secretion by T and NK cells, which further sustains the CCL5–IFN-γ–CXCL9/CXCL10 signaling axis, driving cytotoxic immune cell infiltration and activation [3].

IL-6, conversely, represents a counter-regulatory cytokine often linked to tumor-promoting inflammation and Th2 polarization, providing insight into the inflammatory balance within the tumor microenvironment [45]. Moreover, CCL5, CXCL9, and CXCL10 are frequently epigenetically silenced in certain tumors, and their re-expression restores Th1-type immunity and effector cell infiltration [46]. Thus, these mediators are mechanistically interconnected through CCL5-driven Th1 signaling cascades, and their expression reflects downstream immunological changes resulting from CCL5 modulation.

The rationale for combining CCL5 overexpression with radiotherapy

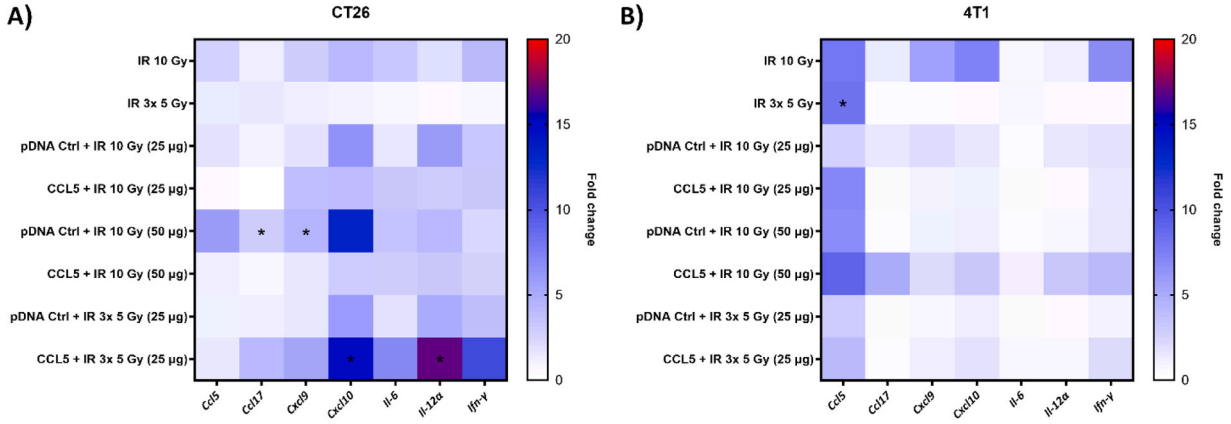

Fig. 3. Gene expression of proinflammatory cytokines in CT26 and 4T1 tumors after GET of pDNA encoding CCL5 and IR. Heat maps show the fold change in expression of inflammatory cytokines (*Ccl5*, *Ccl17*, *Cxcl9*, *Cxcl10*, *Il-6*, *Il-12α*, and *Ifn-γ*) in A) CT26 and B) 4T1 tumors after single-dose IR of 10 Gy, fractionated IR of 3 × 5 Gy, and combined treatments with GET of either pDNA Ctrl or pDNA encoding CCL5 and IR. Cytokine expression was analyzed from tumor tissue homogenates prepared from one half of each collected tumor, and fold change in gene expression was calculated using the ΔΔCt method relative to untreated control tumors collected on day 7. Statistical significance was determined using one-way ANOVA followed by Dunnett's post hoc test, comparing relative expression values of treated groups to the control. A result was considered statistically significant when the average fold increase in gene expression was ≥ 2 and the p-value was < 0.05, as indicated by an asterisk (*). Data represented in the heat maps correspond to the average fold change in gene expression ($5 \leq N \leq 7$). Statistically significant comparisons are summarized in Table S4.

stems from the concept that tumors enriched in effector immune cells generally respond more favorably to radiotherapy and immunotherapy [3]. Because CCL5 is a potent chemoattractant for T lymphocytes, its upregulation through GET delivery could facilitate the increase T-cell infiltration and thereby enhance antitumor responses when used alongside radiotherapy.

In our previous study, expression of proinflammatory cytokines in both tumor models was determined after GET of pDNA Ctrl and GET of pDNA encoding CCL5 alone [31]. In CT26 tumors, GET of control pDNA significantly increased *Il-6* expression at day 3, whereas by day 7, GET of pDNA encoding CCL5 strongly upregulated *Ifn-γ*, *Cxcl9*, *Cxcl10*, *Il-6*, and *Il-12α*. In contrast, 4T1 tumors exhibited only modest, non-significant changes in cytokine expression at both time points.

Expanding upon these earlier findings, we first assessed the effects of irradiation alone. In CT26 tumors, a single-dose IR of 10 Gy alone led to increased expression of *Ccl5* compared to control, which was twice as high compared to fractioned IR (Fig. 3A). The expression of *Ccl17* was lower compared to *Ccl5*, while the expression of all other investigated cytokines increased. Compared to single-dose IR, fractionated IR led to a lower fold change expression of all investigated cytokines, including *Ccl5*. In 4T1 tumors, *Ccl5* expression was increased post-IR regardless of the IR regimen and was about 3 times higher compared to CT26 tumors (Fig. 3A). Increased expression of *Ifn-γ*, *Cxcl9*, and *Cxcl10*, but not of *Il-12α*, was observed after single-dose IR of 10 Gy in 4T1 tumors. Conversely, fractionated IR did not affect the expression of cytokines in 4T1 tumors (Fig. 3B).

When GET of pDNA encoding CCL5 was combined with IR, the expected increase in CCL5 expression was not consistently observed, particularly in CT26 tumors. This effect can be attributed to the relatively high baseline CCL5 expression in CT26, which may have masked additional transgene-driven expression, as well as to the reduced transfection efficiency commonly observed in vivo following GET. In contrast, 4T1 tumors, which exhibit lower basal levels of CCL5, showed clearer upregulation after combination therapy. Nevertheless, both models displayed pronounced modulation of other proinflammatory cytokines and chemokines, likely reflecting the activation of immune pathways triggered by the introduction of plasmid DNA and the electric pulses themselves [47].

Specifically, in CT26 tumors, cytokine expression profiles after combined therapy of GET with 25 μg of pDNA and single-dose IR of 10 Gy were comparable regardless of the pDNA used (Fig. 3A). While combining GET of pDNA Ctrl with single-dose IR increased the expression of *Cxcl10* and *Il-12α*, combining GET of pDNA encoding CCL5 with single-dose IR resulted in comparable upregulation of *Cxcl9*, *Cxcl10*, *Il-6*, *Il-12α* and *Ifn-γ*. In contrast, 4T1 treated tumors showed mainly an upregulation of *Ccl5* (Fig. 3B).

Combining GET using two times higher dose of pDNA (50 μg) and single-dose IR of 10 Gy further potentiated the effect of introduced pDNA Ctrl, resulting in significant upregulation of *Ccl17* and *Cxcl9* in CT26 tumors (Fig. 3A). To a lesser extent this was also observed after GET of pDNA encoding CCL5 and single-dose IR. The most pronounced changes in 4T1 tumors were observed following the combination of GET of pDNA encoding CCL5 with the dose of 50 μg and single-dose IR of 10 Gy. In this treatment group, all cytokines investigated, except Il-6, exhibited more than a 2-fold increase in expression; however, these changes were not statistically significant (Fig. 3B).

Due to the prominent effects of the control pDNA (pDNA Ctrl) on the upregulation of proinflammatory cytokines, GET in combination with fractionated IR was performed using a lower plasmid dose of 25 μg to minimize the effect of the pDNA itself (Fig. 3A and B). When GET with 25 μg of pDNA was combined with fractionated IR 3 × 5 Gy, the most pronounced changes in the expression of all investigated cytokines were observed after GET of pDNA encoding CCL5 in both tumor models (Fig. 3A and B). In CT26 tumors, particularly increased expression of *Cxcl10* and statistically significant expression of *Il-12α* was noted after this therapy (Fig. 3A). Cytokine expression in 4T1 tumors was generally lower compared to CT26 tumors after each combined therapy. As in the case of combined therapies with single-dose IR, combined therapies with fractionated IR also resulted mainly in upregulation of *Ccl5* in 4T1 tumors (Fig. 3B).

3.4. GET of pDNA encoding CCL5 and irradiation results in reduced numbers of tumor infiltrated CD4 + and CD8 + T cells

Given the observed differences in splenocyte migration between the tumor models following therapy, we next assessed the baseline immune status of untreated CT26 and 4T1 tumors (Fig. S2). Tumor sections were stained for cell nuclei, $CD4^+$ and $CD8^+$ T cells, $F4/80^+$ macrophages, and $CD31^+$ endothelial cells, with representative images of each staining shown in Fig. S3. This comparison was performed to characterize the inherent immune landscapes of both models before treatment and to better interpret subsequent therapy-induced changes. Immunofluorescence analyses of untreated mice were conducted on tumor sections collected at day 3 and day 7, corresponding to early and more advanced phases of adaptive immune activation in mice [33]. For treated mice receiving the combination of GET of chemokines and IR, immunofluorescence was performed on tumor sections collected on day 3 after the last IR dose, to capture immune responses during the early post-treatment phase. Both the tumor rim and center were evaluated to capture spatial differences in immune cell distribution, as the rim is typically more vascularized and permissive to infiltration, whereas the center is more hypoxic and immunosuppressive [34].

At baseline, CT26 tumors displayed higher infiltration of $CD8^+$ cytotoxic T cells, while 4T1 tumors contained more $CD4^+$ helper T cells, resulting in an overall lower CD4/CD8 ratio in CT26 (Fig. S2). These findings confirm that CT26 tumors are more immunogenic (“hot”), whereas 4T1 tumors are more immunosuppressive (“cold”), consistent with previously published data [31]. The tumor vascular area did not significantly differ between the models at baseline.

The tumor vascular area was quantified because radiotherapy is known to markedly remodel tumor vasculature through vessel loss, pruning, or normalization, and these changes can directly influence immune-cell trafficking into tumors. Measuring vascular area therefore allows interpretation of immune-cell infiltration—particularly CCL5-driven T-cell recruitment—in the context of radiation-induced vascular alterations, rather than attributing all differences solely to chemokine effects [48–50]. This is particularly relevant for CCL5 because chemokine-mediated lymphocyte recruitment requires a functional vascular network for circulating cells to extravasate into the tumor.Following the characterization of baseline immune profiles, we next examined how GET of pDNA encoding CCL5 combined with IR affects immune-cell infiltration. Regardless of the plasmid dose the most significant changes in immune cell populations after GET of pDNA encoding CCL5 and IR were observed at the tumor rims (Fig. 4), while the tumor centers exhibited a similar trend, though less pronounced (Fig. S4).

In CT26 tumors single-dose IR of 10 Gy did not change the number of CD4 + T cells at the tumor rims, while the number of CD8 + T cells slightly decreased compared to the control (Fig. 4A Figs. S5Ai and Aii). On the contrary, in 4T1 tumors single-dose IR with 10 Gy led to a reduction in CD4 + and a 64.5 % increase in the mean number of CD8 + T cells (Fig. 4B, Figs. S6Ai and Aii). In CT26 tumors, the number of CD8 + T cells decreased after all combined therapies with single-dose IR (Fig. 4C, E, Figs. S5Ai-Bii). Reduced immune cell infiltration was also observed in 4T1 tumors following combined therapies with single-dose IR (Fig. 4D, F, H, Figs. S6Ai-Bii). F4–80 + macrophages were primarily observed at the tumor rims, and were not significantly affected by the therapies in both tumor models (Fig. 4A-H).

In contrast to single-dose IR, fractionated IR of 3 × 5 Gy in CT26 tumors increased the infiltration of CD4 + and CD8 + T cells, particularly at the tumor rims (Fig. 4A, Figs. S5Ci and Cii). Despite this, GET of pDNA encoding CCL5 combined with fractionated IR led to a significant

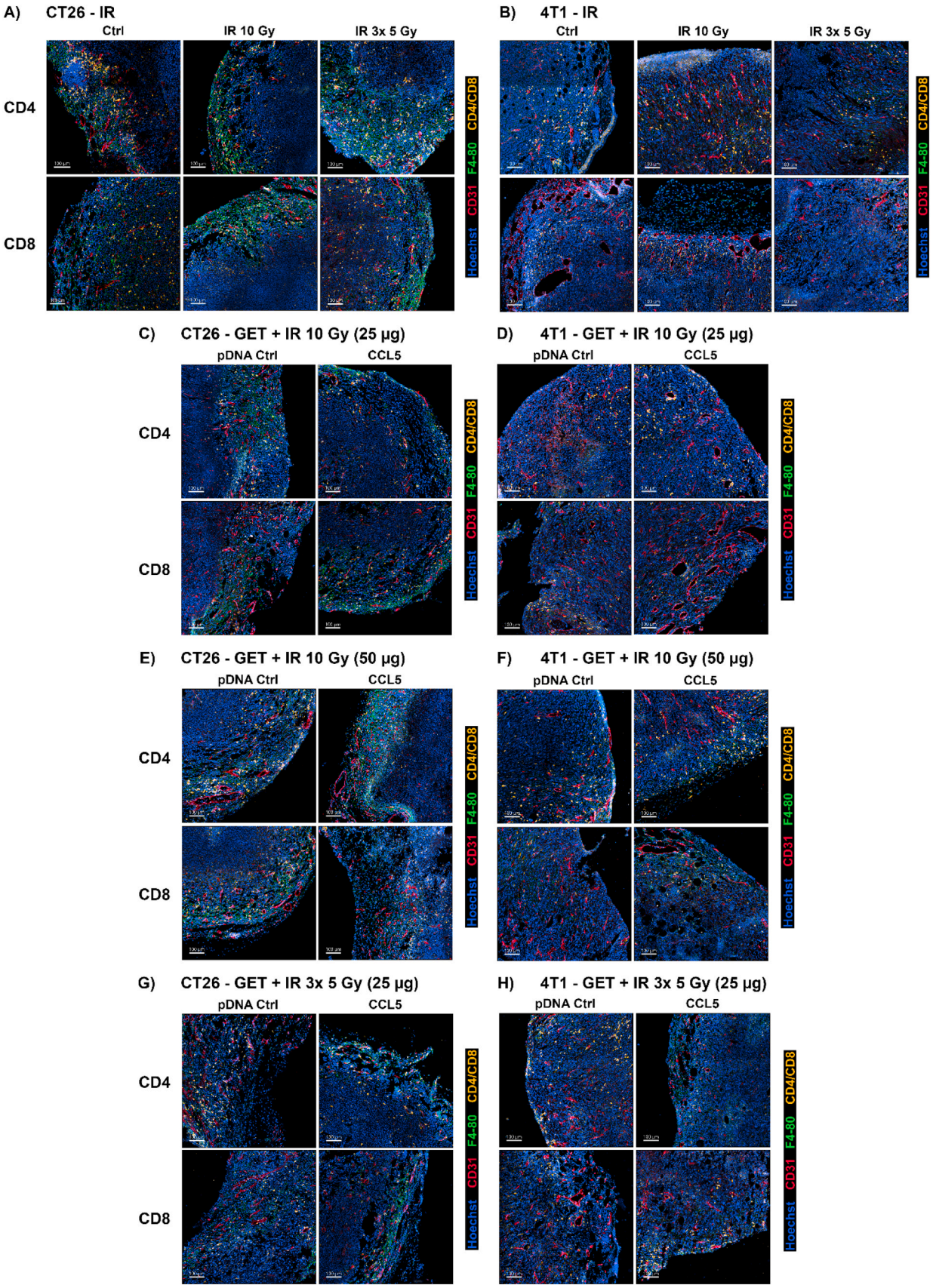

(caption on next page)

Fig. 4. Representative immunofluorescence images of CT26 and 4T1 tumor rims after GET of pDNA encoding CCL5 and IR. Frozen tumor sections were labeled with anti-CD4 or anti-CD8 (yellow, Cy3), anti-CD31 (red, Alexa 647), anti-F4–80 (green, Alexa 488), and Hoechst 33342 (blue). Representative immunofluorescence images show immune cell populations at the rims of CT26 and 4T1 tumors. Images A) and B) present tumors treated with single-dose IR of 10 Gy and fractionated IR of 3 × 5 Gy in CT26 tumors (A) and 4T1 tumors (B), respectively. Images C) and D) show tumors following combined treatment of GET with 25 μg of either pDNA Ctrl or pDNA encoding CCL5 and single-dose IR of 10 Gy in CT26 (C) and 4T1 (D) tumors. Images E) and F) show tumors following the same treatment groups using 50 μg of pDNA and single-dose IR of 10 Gy in CT26 (E) and 4T1 (F) tumors. Images G) and H) show tumors following combined treatment of GET with 25 μg of either pDNA encoding CCL5 or pDNA Ctrl and fractionated IR of 3 × 5 Gy in CT26 (G) and 4T1 (H) tumors. Images of tumors following single-dose and fractionated IR were acquired on day 7 after treatment, while images of combined treatments were acquired on day 3 after the last IR dose (N = 5). Yellow: CD4/CD8; red: CD31; green: F4/80; blue: cell nuclei. Scale bar: 100 μm.

decrease in both immune populations in tumors (Fig. 4G, Figs. S5Ci and Cii). In 4T1 tumors fractionated IR reduced the number of CD4 + T cells, but did not affect the number of CD8 + T cells (Fig. 4B, Figs. S6Ci and Cii). Combined therapies did not significantly reduce the number of CD4 + or CD8 + T cells and were preserved at higher numbers in 4T1 tumors compared to CT26 tumor model. Due to the changes in the numbers of CD4 + and CD8 + T cells after the combined therapies, the CD4/CD8 T cell ratio was proportionally affected (Figs. S5Di, Ei, Fi, S6Di, Ei, and Fi). Significantly increased CD4/CD8 T cell ratio in CT26 tumors was observed also after combined treatment of GET of pDNA encoding CCL5 and 3 × 5 Gy (Fig. S5Fi). In case of 4T1 tumors CD4/CD8 T cell ratio was not significantly affected after therapies.

Up to 50 % reduction (from ≈6 % to ≈3 %) in the tumor vascular area represented by CD31 + endothelial cells was observed at CT26 tumor rims after single-dose IR and combined therapies of GET of pDNA encoding CCL5, while after GET of pDNA Ctrl, the vessels were mostly

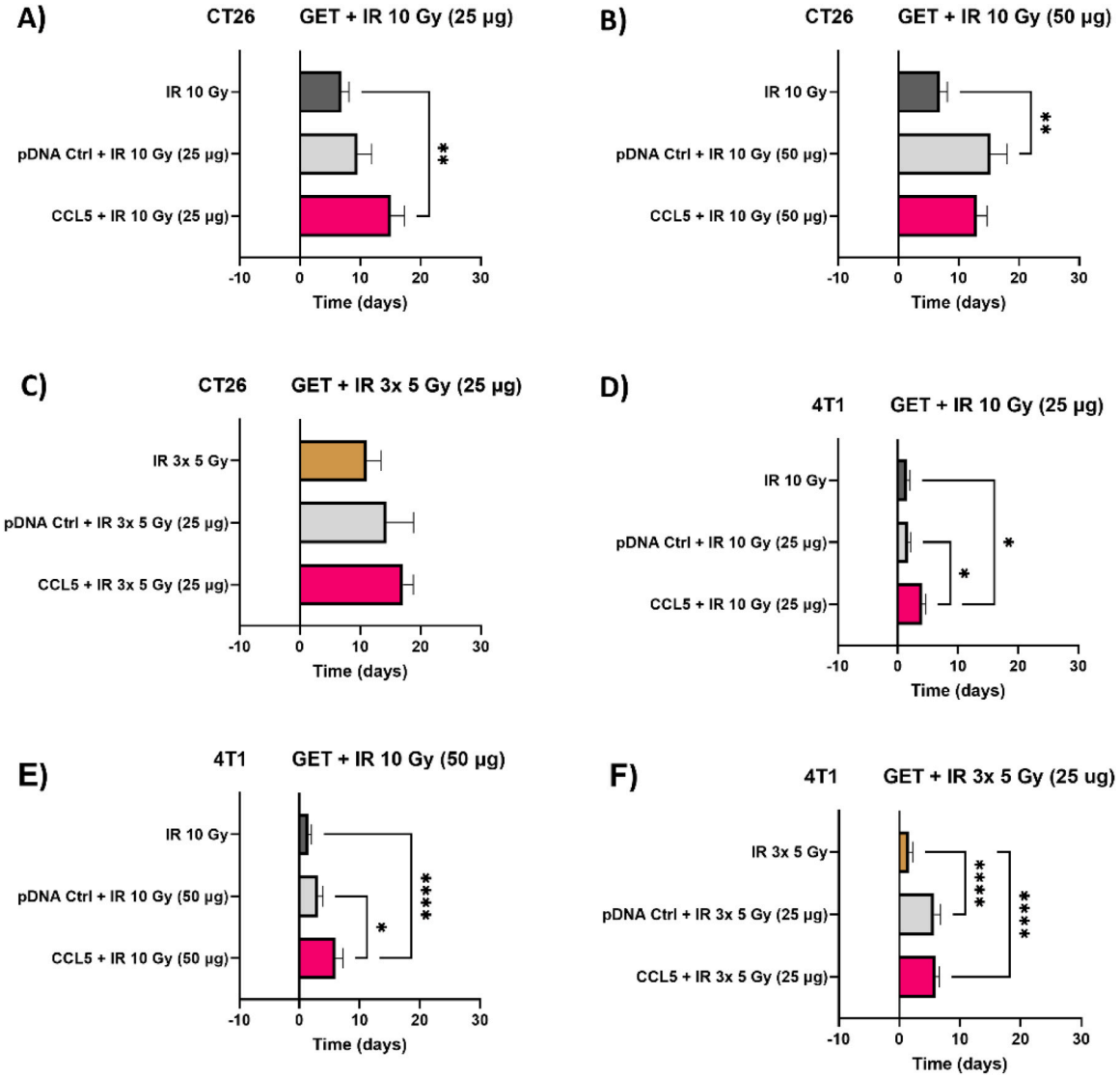

Fig. 5. Tumor growth delays of CT26 and 4T1 tumors after GET of pDNA encoding CCL5 and IR. Graphs show tumor growth delays of CT26 and 4T1 tumors after combined therapies. Graphs A-C) correspond to CT26 tumors, and graphs D-F) to 4T1 tumors. Graphs A) and D) present tumor growth delay following GET with 25 μg of either pDNA Ctrl or pDNA encoding CCL5 and single-dose IR of 10 Gy. Graphs B) and E) show tumor growth delay following the same treatment groups using 50 μg of pDNA. Graphs C) and F) display tumor growth delay after GET with 25 μg of either pDNA Ctrl or pDNA encoding CCL5 and fractionated IR of 3 × 5 Gy. Data are expressed as AM ± SEM of all mice ($17 \leq N \leq 35$). Statistical significance was determined by ordinary one-way ANOVA. A p-value of < 0.05 was considered statistically significant (*$p < 0.05$, **$p < 0.01$, ****$p < 0.0001$ between groups).

preserved (Figs. S5Dii and Eii). In the case of fractionated IR, the percentage of vascular area at the tumor rims and inside was significantly lower only after combined treatment with GET of pDNA encoding CCL5 (Fig. S5Fii). Similar, but not statistically significant changes in the tumor vascular area were observed in treated 4T1 tumors (Figs. S6Dii, Eii and Fii).

Lastly, we determined the distances between the immune cells and tumor vessels. In CT26 tumors CD4 + T cells were located the farthest from the vasculature at the rims of CT26 tumors after single-dose IR with 10 Gy (Figs. S7Ai, Bi, and Ci), while the average distance of CD4 + T cells after all combined therapies was approximately 5 μm. The distances of CD8 + T cells to tumors vessels fluctuated between therapies but did not statistically differ compared to control (Figs. S7Aii, Bii, and Cii). Although combined therapies with fractionated IR did not affect the distance of CD4 + T cells from the vessels, the furthest distance of CD8 + T cells from the vessels was observed after GET with 25 μg of pDNA encoding CCL5 combined with fractionated IR (Fig. 4 Ci and Cii). In 4T1 tumors GET of pDNA Ctrl combined with fractionated IR led to significantly reduced distance between CD8 + T cells and tumor vessels (Figs. S8Ai-Cii).

3.5. GET of pDNA encoding CCL5 combined with irradiation leads to tumor immune status–specific responses in mice

In the immunogenic CT26 tumors, the results of determining the tumor growth delay after GET of pDNA encoding CCL5 and IR showed that tumors respond to the combined therapy (Fig. 5A-C). Single-dose IR of 10 Gy alone did not lead to complete responses (CRs), although the tumor growth delay was significantly longer relative to the control, amounting to 6.9 ± 1.2 days (Table S5; row 1). The tumors had the longest growth delay after GET with 25 μg of pDNA encoding CCL5 and single-dose IR, which was 15.0 ± 2.3 days with 35 % of CRs, however the difference compared to the GET of pDNA Ctrl was not statistically significant (Fig. 5A, Table S5; rows 3 and 4). In the tumor regrowth experiment, 50 % of tumors treated with GET of pDNA encoding CCL5 grew back. Survival of the mice was significantly longer for all treatment groups compared to control (Fig. 6A).

Even in the case of GET with 50 μg pDNA, the highest number of CRs was observed following GET of pDNA encoding CCL5 and single-dose IR, although the tumor growth delays were comparable between the treatment groups (Fig. 5B). GET of pDNA Ctrl and single-dose IR led to 7.7 % CRs, while GET of pDNA encoding CCL5 resulted in 22.2 % CRs (Fig. 6B, Table S5; rows 5 and 6). The tumor regrowth experiment showed that immune memory developed particularly in mice with cured CT26 tumors treated with GET of pDNA encoding CCL5 and single-dose

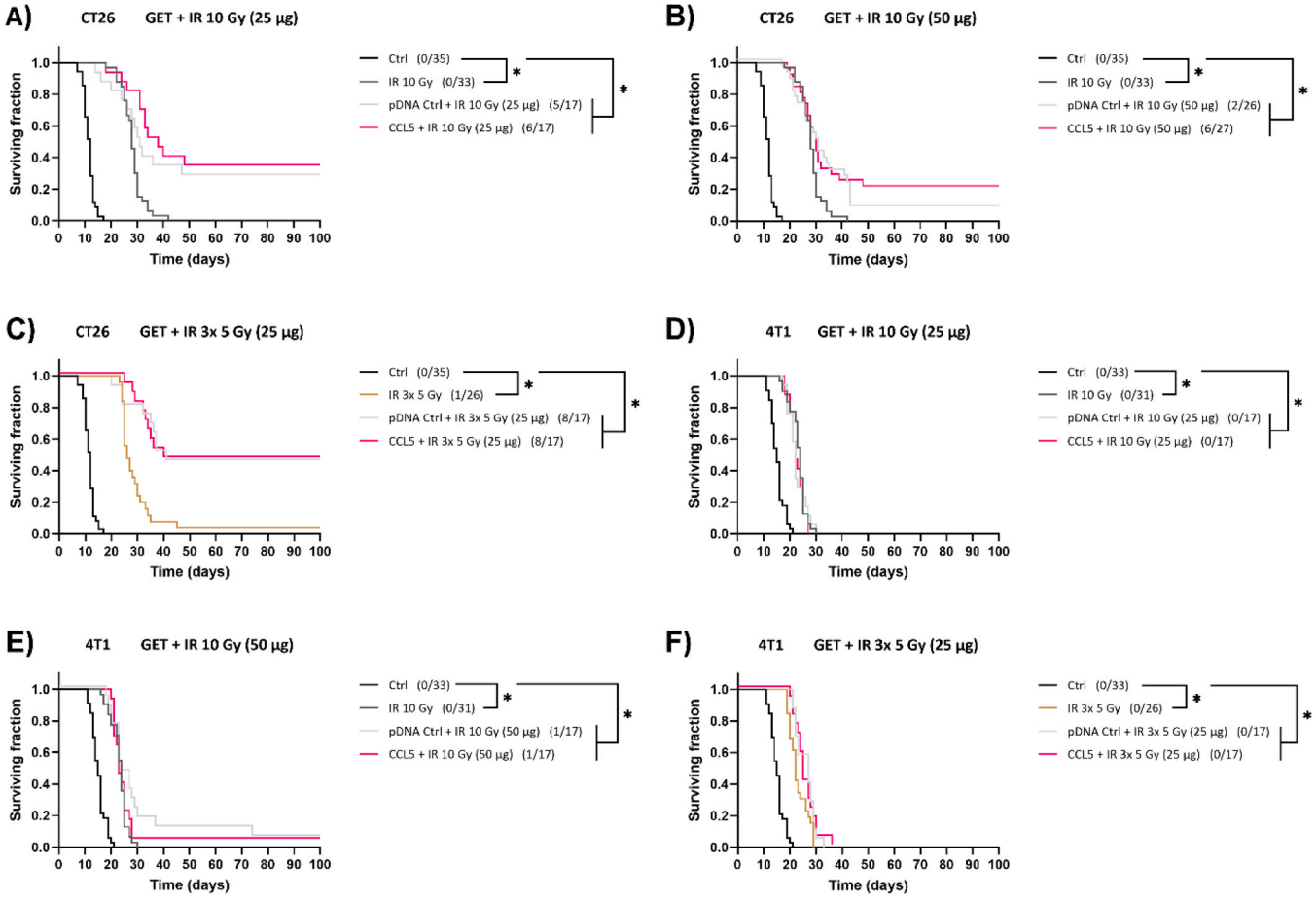

Fig. 6. Survival of mice bearing CT26 and 4T1 tumors after GET of pDNA encoding CCL5 and IR. Kaplan–Meier survival curves show outcomes for mice bearing CT26 and 4T1 tumors over 100 days. Graphs A-C) correspond to mice bearing CT26 tumors, and graphs D-F) to mice bearing 4T1 tumors. Graphs A) and D) present survival following GET with 25 μg of either pDNA Ctrl or pDNA encoding CCL5 and single-dose IR of 10 Gy. Graphs B) and E) show survival of the same treatment groups using 50 μg of pDNA. Graphs C) and F) show survival following GET with 25 μg of either pDNA Ctrl or pDNA encoding CCL5 and fractionated IR of 3 × 5 Gy. Numbers in parentheses after each group represent the number of complete responses (CRs) and the total number of mice in the corresponding group ($17 \leq N \leq 35$). Statistical significance was determined by Log-rank test with Holm–Šidák correction for multiple comparisons. A p-value of < 0.05 was considered statistically significant (*$p < 0.05$ between groups).

IR, as only 20 % of tumors regrew after rechallenge (Table S5; row 6).

Fractionated IR of 3 × 5 Gy alone resulted in 3.8 % CRs in CT26 tumors, while the tumor growth delay was significantly longer relative to the control, amounting to 11.0 ± 2.4 days (Table S5; row 2). GET with 25 μg of pDNA Ctrl and fractionated IR resulted in 47.1 % CRs and tumor growth delay of 14.3 ± 4.5 days (Fig. 5C, Table S5; row 7). Similarly, GET with 25 μg of pDNA encoding CCL5 and fractionated IR led to 47.1 % CRs and tumor growth delay of 17.1 ± 1.7 days (Fig. 5C, Table S5; row 8). Immune memory developed in 33 % of mice receiving GET of pDNA Ctrl, whereas GET of pDNA encoding CCL5 led to tumor resistance in 50 % of treated mice (Table S5; rows 7 and 8). The survival of mice was comparable between the two treatment groups (Fig. 6C).

In the non-immunogenic 4T1 tumors, the tumor growth delay after GET of pDNA encoding CCL5 and IR showed that 4T1 tumors were less responsive to the combined therapy compared to CT26 tumors (Fig. 5D-F). Single-dose IR of 10 Gy did not lead to CRs, while the tumor growth delay was significantly longer relative to the control, amounting to 1.5 ± 0.4 days (Table S6; row 1). The tumors had the longest growth delay after GET with 25 μg of pDNA encoding CCL5 and single-dose IR, which was 4.0 ± 0.6 days (Figs. 5D and 6D, Table S6; rows 3 and 4). Although no CRs were observed, the combined GET of pDNA encoding CCL5 and single-dose IR showed a significantly longer tumor growth delay relative to the GET of pDNA Ctrl and single-dose IR and a significantly longer survival of the mice compared to the control (Figs. 5D and 6D). Specifically, the tumor growth delay was approximately 2.5 times longer compared to the GET with 25 μg of pDNA Ctrl. Similar trend was observed for the therapies with the higher amount of pDNA (Figs. 5E and 6E, Table S6; rows 5 and 6). In this case each combined therapy resulted in one CR (5.9 %) in the treated groups; however, immune memory did not develop in the cured mice, as all tumors regrew in the rechallenge experiment (Table S6; rows 5 and 6).

Fractionated IR of 3 × 5 Gy alone did not lead to CRs in 4T1 tumors, while the tumor growth delay amounted to 1.6 ± 0.7 days (Table S6; row 2). GET with 25 μg of pDNA Ctrl and fractionated IR resulted in tumor growth delay of 5.7 ± 1.1 days (Fig. 5F, Table S6; row 7) while, GET with 25 μg of pDNA encoding CCL5 and fractionated IR resulted in tumor growth delay of 6.0 ± 0.6 days (Fig. 5F, Table S6; row 8). None of the treatments led to CRs (Table S6; rows 7 and 8). The survival of the mice was comparable across all treatment groups (Fig. 6C).

Given the observed reduction in CD4 + and CD8 + T cells in our immunofluorescence analysis after combined treatments and the potential immune cell depletion caused by IR, we performed a double GET with 25 μg of pDNA combined with fractionated IR of 3 × 5 Gy (Fig. S9). In this approach, a second GET was administered 24 h after the final IR dose to preserve and potentially enhance immune cell infiltration. Notably, double GET combined with fractionated IR increased the expression of introduced CCL5, while the expression levels of other cytokines remained at basal levels (Figs. S9A and B). In CT26 tumors, tumor growth delay was significantly longer relative to controls, though the effect of pDNA masked the specific contribution of CCL5 (Figs. S9C and D). In 4T1 tumors, growth delay after GET of pDNA encoding CCL5 reached 8.6 ± 1.6 days, which was significantly longer than in both control groups. However, in both tumor models, the survival of mice was not improved and the number of CRs was lower compared to combined treatments with single GET (Figs. S9E and F).

Tumor response to combined therapies was further assessed by comparing normalized tumor doubling times and DRAP analysis [42] between CT26 and 4T1 tumors (Fig. 7). All therapies significantly prolonged doubling times in CT26 tumors compared to 4T1. Fractionated IR and GET combined with fractionated IR led to longer doubling times in CT26, though response variability was higher (Figs. 7Ai-Aiii). Violin plot distribution showed that only a fraction of CT26 tumors exhibited increased number of tumor doublings, while 4T1 tumors showed comparable responses, indicating lower inter-tumor heterogeneity (Figs. 7Ai-Di and 7Aii-Dii).

In CT26 tumors, both IR regimens led to 15.4 % stable disease (SD) responses (Fig. 7Aiii), whereas in 4T1 tumors, only progressive disease (PD) was observed. Fractionated IR in CT26 tumors also doubled the rate of partial responses (PR) to 7.7 % compared to single-dose IR. When combining GET with 25 μg pDNA and single-dose IR, CT26 tumors showed improved responses: GET of pDNA resulted in 11.8 % PR and 11.8 % SD, while GET of pDNA encoding CCL5 increased these outcomes to 17.6 % PR and 29.4 % SD (Fig. 7Biii). In contrast, the same treatment in 4T1 tumors yielded only PD. GET with 50 μg of pDNA encoding CCL5 combined with single-dose IR in CT26 tumors further raised the SD rate by 10.1 % and reduced PR by 15.7 % compared to pDNA Ctrl (Fig. 7Ciii). Interestingly, in 4T1 tumors, GET of pDNA Ctrl led to 11.8 % more PR than GET of pDNA encoding CCL5. Finally, in CT26 tumors, GET of pDNA encoding CCL5 combined with fractionated IR resulted in 5.9 % more PR and 11.7 % more SD than the corresponding pDNA Ctrl treatment (Fig. 7Diii).

4. Discussion

Exploiting chemokines represents an emerging therapeutic strategy in oncology due to their ability to attract and guide immune cells. In our previous study, the antitumor effect of GET of pDNA encoding CCL5 as a monotherapy has been evaluated [31]. Although overexpression of CCL5 and other proinflammatory cytokines after GET was observed, the therapy led only to a minor tumor growth delay. Therefore, in this study the effect of GET of pDNA encoding CCL5 in vivo was combined with radiotherapy to potentiate the antitumor effectiveness. Specifically, we determined the antitumor efficacy of chemokine CCL5 gene therapy utilizing gene electrotransfer (GET) in combination with radiotherapy (RT) in solid murine tumors CT26 and 4T1. These findings highlight the potential of CCL5 gene therapy via GET in combination with RT as a promising strategy for enhancing immune-mediated tumor control.

The comparison between single-dose IR of 10 Gy and fractionated IR of 3 × 5 Gy was included to explore how different dose delivery schedules influence the therapeutic synergy with CCL5. These regimens were chosen because they deliver the same biologically effective dose (BED), assuming an α/β ratio of 10 for early-responding tissues such as tumors [41]. This allowed us to determine whether a single high dose or a fractionated dosing schedule provides greater therapeutic benefit when combined with CCL5 overexpression. Differences in dose delivery—one-time IR versus repeated exposures over three consecutive days—can affect tumor cell repair capacity, the kinetics of immune activation, and the overall composition of the tumor microenvironment [51].

The chemotactic ability of CCL5 was initially investigated using an in vitro migration assay, where we demonstrated that CT26 and 4T1 tumor cells transfected with pDNA encoding CCL5 significantly enhanced the migration of RAW264.7 macrophages. Although GET is a simple and effective method for delivering pDNA into tumors and tissues in vivo, its main drawbacks are variability in transfection efficiency and its impact on viability among different cell lines and electric pulse protocols in vitro [52,53]. Additionally, electric pulses themselves can influence the expression of different genes [54–56]. For these reasons, CT26 and 4T1 tumor cells used in in vitro chemotaxis assays were transfected with pDNA encoding chemokine CCL5 and control, non-coding pDNA (pDNA Ctrl) using lipofection, which is known as highly efficient and low cytotoxic transfection method for in vitro transfection [57].

In addition to macrophage migration, T-cell chemotaxis was assessed in vitro using CTLL-2 lymphocytes together with CT26 or 4T1 cells transfected with pDNA encoding CCL5 via lipofection. Because CTLL-2 cells are non-adherent suspension cells, migration was evaluated using Boyden transwell assays. However, results were inconsistent due to the sensitivity of these cells, instability of CCL5 gradients, and technical variability. Therefore, these data were not included, and T-cell recruitment was instead analyzed in vivo, where chemokine gradients and physiological conditions are more stable.The highest rate of macrophage migration was observed towards tumor cells transfected with pDNA

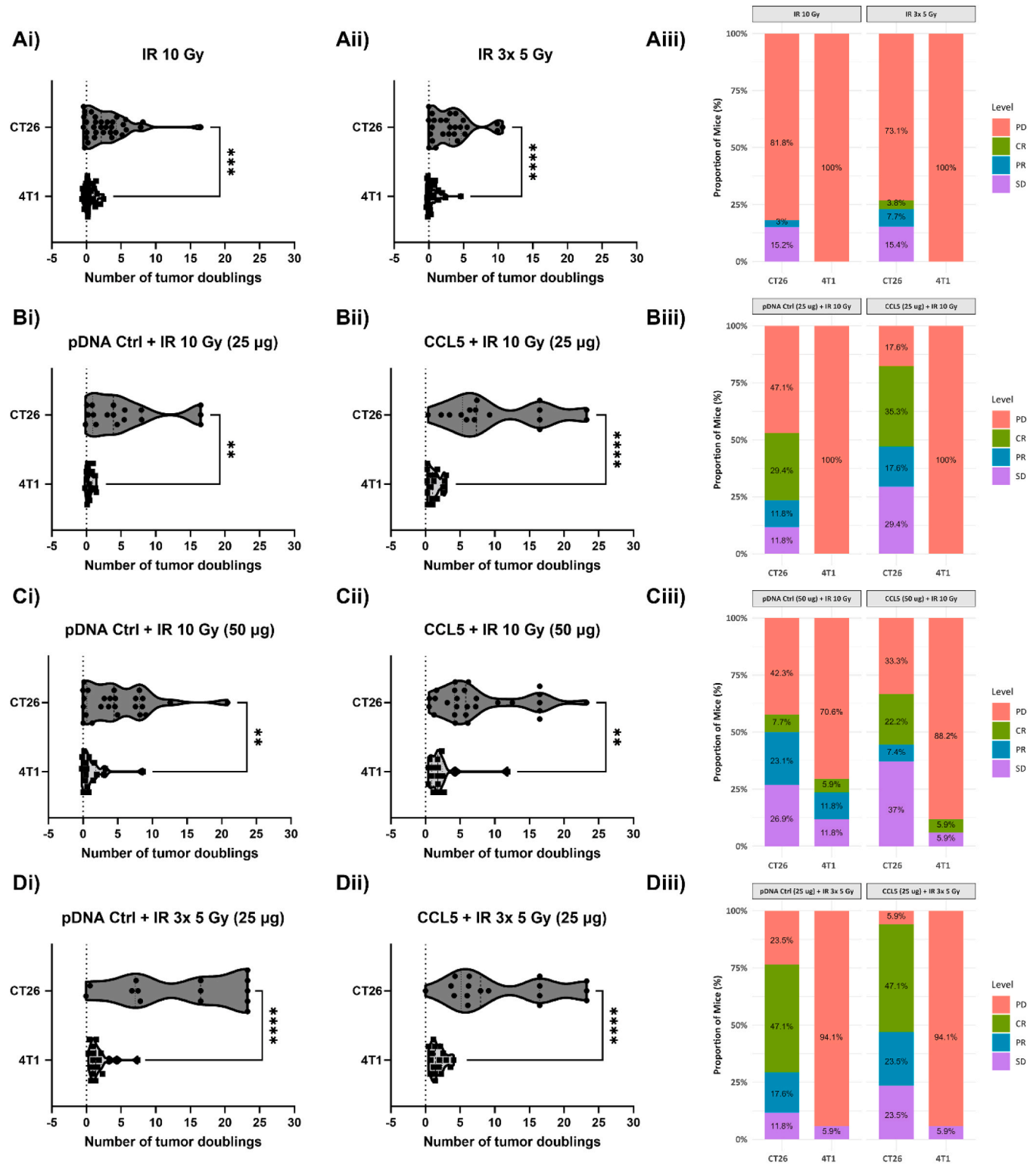

Fig. 7. Treatment response comparison of CT26 and 4T1 tumors after combined therapies. Graphs Ai-Dii) the number of tumor doublings of CT26 and 4T1 treated with single-dose IR of 10 Gy (Ai), fractionated IR of 3 × 5 Gy (Aii), GET with 25 µg of pDNA Ctrl (Bi) or pDNA encoding CCL5 (Bii) combined with IR 10 Gy, GET with 50 µg of pDNA Ctrl (Ci) or pDNA encoding CCL5 (Cii) combined with IR 10 Gy and GET with 25 µg of pDNA Ctrl (Di) or pDNA encoding CCL5 (Dii) combined with fractionated IR 3 × 5 Gy. The data show the difference in doubling time relative to control, presented as violin plots and expressed as AM ± SEM of all mice ($17 \leq N \leq 33$). A p-value of < 0.05 was considered statistically significant (*$p < 0.05$, **$p < 0.01$, ****$p < 0.0001$ between tumor models). Drug response plots Aiii–Diii) were generated using the DRAP tool with tumor volume measurements as input data. The plot represents the proportion of mice corresponding to each response category, as determined by NPDX criteria: PD: progressive disease (red); CR: complete response (green); PR: partial response (blue); and SD: stable disease (magenta).

encoding CCL5. This outcome was expected, as CCL5 functions by binding to CCR1, CCR3, CCR5 receptors, which are abundantly expressed by RAW264.7 macrophages as determined with high-throughput sequencing (Yao M, data accessible at NCBI GEO database, accession GSE271238). Moreover, this also served to validate the effectiveness of the pDNA transfection in tumor cells used in our study. Over the 20-hour period, an increase in the number of migrating macrophages towards CT26 cells was observed, eventually reaching a plateau in all groups. This plateau may indicate receptor desensitization and a subsequent stall in migration [58], a process that occurs to prevent overstimulation of signaling pathways and maintain cellular homeostasis by diminishing receptor responsiveness following prolonged or repeated exposure to a ligand.

Interestingly, an even stronger effect was observed in macrophage migration toward pDNA Ctrl-transfected CT26 cells, suggesting that the presence of foreign non-coding DNA might activate pathways that disrupt endogenous chemotactic gradients of transfected CT26 cells. Indeed, this could be due to the upregulation of numerous proinflammatory cytokines, as previously demonstrated in murine colon (CT26, MC38) and breast cancer (4T1, E0771) cell lines following lipofection with pDNA Ctrl [31].

All transfected 4T1 cells induced significantly higher linear migration trend of macrophages, with pDNA encoding CCL5 inducing the highest difference, in comparison to the control group. Unlike in CT26 cells where macrophage migration caused by non-coding pDNA was comparable to untreated control, in 4T1 cells pDNA Ctrl induced a significant increase in macrophage migration. This difference could be attributed to the distinct phenotypes of CT26 and 4T1 cells characterized by different cytokine baseline states [59]. CT26 cells are known to form immunogenically active, "hot" tumors characterized by high infiltration of NK cells (>26 %) and T lymphocytes (>18 %), with cytotoxic T lymphocytes making up more than 5 % of the infiltrate [60]. In contrast, 4T1 cells form non-immunogenic, immunosuppressive tumors with high infiltration of regulatory T (Treg) lymphocytes (>5 %) and myeloid-derived suppressor cells (MDSCs, >50 %), alongside increased Th2-associated cytokine signaling.

These intrinsic differences were also evident in our immunofluorescence analysis of untreated tumors, where CT26 tumors contained fewer $CD4^+$ but more $CD8^+$ T cells and exhibited a lower CD4/CD8 ratio compared to 4T1. The CD4/CD8 ratio provides additional insight into how CCL5 may modulate the composition of infiltrating lymphocytes. While both $CD4^+$ and $CD8^+$ T cells can respond to CCL5, their chemotactic sensitivity differs—$CD8^+$ and activated/memory T cells generally express higher levels of CCR5, the principal receptor for CCL5, than $CD4^+$ T cells. Consequently, alterations in this ratio may indicate preferential recruitment of cytotoxic T-cell subsets and reflect a shift toward a more effective antitumor immune microenvironment. Together, these findings underscore the distinct immune landscapes of CT26 and 4T1 tumors and their likely influence on therapeutic outcomes.

To further investigate the chemotactic properties of CCL5 in vivo, its chemotactic properties were determined also using DWCs of CT26 and 4T1 tumors through observation of naïve splenocyte infiltration into the TME. To achieve this, GET of pDNA encoding CCL5 was performed using established electrical pulses used in clinics for electrochemotherapy [38,39]. The results at 24- and 48-hour time point demonstrated that CCL5-transfected tumors after GET led to increased splenocyte infiltration in both tumor models. Notably, in non-immunogenic 4T1 tumor model the splenocyte recruitment was significant compared to control, suggesting that GET of pDNA encoding CCL5 can effectively override the immunosuppressive nature of these tumors. While the number of intratumoral splenocytes significantly increased after the therapy, the number of peritumoral splenocytes remained unchanged. This is likely due to a combination of immune cell retention within the tumor as a consequence of establish chemokine CCL5 gradients, as well as structural and functional characteristics of the TME at the periphery [61,62], and the side effects of electric pulses delivered during GET [63,64]. However, a limitation of this study is that while changes in the number of splenocytes were observed, the detailed mechanisms underlying these localized effects, such as specific chemokine expression or individual immune cell tracking in the DWCs were not investigated and warrant further studies.

Collectively, the introduction of non-coding, foreign pDNA in CT26 tumors did not significantly affect macrophage migration rates, while its presence in 4T1 cells caused a notable shift, turning these typically non-immunogenic tumor cells into cytokine producers and substantially increasing macrophage migration compared to the control. Although the effect of non-coding pDNA decreased, at later time points, 4T1 cells transfected with pDNA encoding CCL5 continued to drive substantial macrophage migration. Similarly, in vivo evaluation using DWCs demonstrated that the effects of control pDNA were limited, while GET of pDNA encoding CCL5 significantly enhanced splenocyte recruitment, particularly in the immunosuppressive 4T1 tumor model. This splenocyte infiltration was significant, suggesting the establishment of chemokine gradients and enhanced immune cell retention within the TME. These findings highlight the distinct effects of GET of pDNA encoding CCL5, which not only enhance macrophage and splenocyte recruitment but also effectively override the immunosuppressive nature of 4T1 tumors, maintaining their pronounced effects even as the influence of non-coding pDNA subsides.

The efficacy of chemokine CCL5 gene therapy utilizing GET in combination with RT in solid murine tumors CT26 and 4T1 was stratified across multiple levels, including gene expression analysis of proinflammatory cytokines, immune cell infiltration, and determination of responses after therapies. Single-dose IR of 10 Gy alone increased the production of proinflammatory cytokines *Ccl5*, *Cxcl9*, *Cxcl10* and *Ifn-γ*, while fractionated IR of 3×5 Gy did not. Different single-dose and fractionated IR regimens have been shown to elicit divergent immunological outcomes, with the dose and scheduling influencing the magnitude, quality, and timing of cytokine responses, which may also differ between tumor models [65,66]. Studies indicate that elevated expression of *Cxcl9* and *Cxcl10* correlates with the degree of infiltrating CD4 + and CD8 + T cells, activation of Th1 cells in the TME, and effectiveness of immunotherapies [3,67]. Meta-analysis in murine ovarian tumors also showed correlation between high expression of cytokines *CCL5*, *CXCL9*, *IFN-γ*, and better response to treatment with immune checkpoint inhibitors in patients with various cancers. This suggests that combined therapy with GET pDNA encoding CCL5 in combination with RT could contribute to a greater anti-tumor efficacy. Furthermore, epigenetic studies in mice show that *Ccl5*, *Cxcl9*, and *Cxcl10* are epigenetically silenced [46,68], and that IFN-γ-mediated signaling is suppressed in immunosuppressive tumors such as 4T1 [59,69]. Restoring the expression of those epigenetically silenced genes could promote Th1 cell activation and trigger effector immune cell infiltration.

In our study, gene expression analysis of CT26 tumors showed that most of investigated combined therapies of GET and IR predominantly led to an increased expression of *Cxcl9*, *Cxcl10*, *Il-6*, *Il-12α* and *Ifn-γ*. IL-12 is known to further activate and enhance the cytotoxic activity of CD8 + T cells, NK cells, inhibit or reprogram immunosuppressive cells, and induce IFN-γ production [70–72]. While increased expression of these cytokines following combined therapies could be attributed to Th1 immune response activation, secretion of IL-6 is associated with major tumor characteristics and activation of Th2-type immune response, which could inhibit anti-tumor immune response and facilitate tumor progression [45,73,74]. In 4T1 tumors, combined therapies generally led to an increase in *Ccl5*, while GET of pDNA encoding CCL5 combined with single-dose IR of 10 Gy also resulted in increased expression of other proinflammatory cytokines, including *Ccl5, Ccl17, Cxcl9, Cxcl10, Il-12α, Ifn-γ*, but not *Il-6*. Although our combined therapy shifted the equilibrium of both tumor models toward “hot”, immunologically active tumors, statistical significance was limited, likely due to tumor heterogeneity. Moreover, further in-depth transcriptomic studies in treated

tumors are needed to comprehensively characterize the cytokine expression profiles following GET of pDNA encoding CCL5.

An additional limitation of this study is that cytokine and chemokine expression after combined therapies was assessed only at the mRNA level. Future studies should therefore include complementary protein analyses to better validate and interpret the transcriptional changes observed here.

Nevertheless, these cytokine expression profiles were indicative of increased CD4 + and CD8 + T cell populations within the TME, which were determined in the subsequent step by immunofluorescence staining of frozen tumor sections after combined treatments. Immune cell populations in CT26 and 4T1 tumors after combined therapies were assessed on day 3 after the final IR dose using immunofluorescent staining. The analysis showed that CD4 + and CD8 + T cell numbers either remained comparable to controls or decreased. This reduction could be attributed to the direct effects of IR, which can induce cell death in radiation-sensitive immune cells. In this study, both single-dose and fractionated IR were designed to deliver the same biologically effective dose (BED ≈ 22 Gy). These moderately high doses effectively damage tumor and stromal cells but can also transiently reduce lymphocyte abundance within the tumor microenvironment, particularly shortly after the final irradiation.

However, a limitation of the study was that CD4 + , CD8 + , and F4/80 + immune cell populations were evaluated only at a single time point. The chosen time point (day 3 post-IR) was selected to align with the onset of immune cell activation following therapy in mice [43]. At this stage, radiation-induced cytotoxicity and vascular remodeling may still outweigh later immune recruitment processes typically triggered by IR. Later time points were considered less suitable because significant tumor regression in responder mice would render the tumors too small for meaningful analysis, thereby limiting the availability of adequate samples. While delaying the initiation of treatment until tumors reach a larger volume (e.g., ≥50 mm^3, as in this study) might mitigate this issue, it carries the risk of developing necrotic centers within the tumors [75].

The observed reduction in T-cell numbers also appeared to differ between tumor types. In CT26 tumors, which are immunogenic and rich in pre-existing effector cells, IR likely caused depletion of infiltrated $CD4^+$ and $CD8^+$ T cells and transient suppression of chemokine-driven recruitment. This interpretation is consistent with cytokine expression data showing increased *Cxcl9*, *Cxcl10*, and *Il-12α* levels following combined treatments, suggesting activation of Th1-type signaling without yet translating into measurable T-cell accumulation at this time point. In contrast, the 4T1 model, characterized by a strongly immunosuppressive microenvironment and high baseline levels of MDSCs and Tregs, showed limited changes in immune infiltration. Here, IR primarily induced upregulation of *Ccl5*, but not of *Cxcl9* or Cxcl10, indicating that the chemokine gradients required for robust lymphocyte recruitment were not sufficiently established.

Another possible explanation for the reduced immune cell infiltration would be that IR induced cell death contributes to lower expression of introduced chemokines [76]. This reduction in CCL5 transgene expression may have been more pronounced in CT26 tumors, where transfection efficiency and baseline chemokine levels were already high, masking additional CCL5-mediated effects. This could prevent the establishment of sufficient chemokine gradients, thereby limiting immune cell infiltration. However, this is less likely considering the observed tumor growth delay and treatment outcomes after combined therapies.Overall, these findings suggest that the decrease in $CD4^+$ and $CD8^+$ T-cell numbers reflects the cytotoxic and transcriptional consequences of IR within distinct tumor immune landscapes—acute depletion in immunogenic CT26 and persistent exclusion in immunosuppressive 4T1—rather than contradicting the established concept that radiotherapy promotes immune infiltration at later stages. Future work including later analysis time points or partial-tumor IR strategies may better capture the kinetics of immune recruitment and help clarify these model-dependent dynamics.

While single-dose IR and fractionated IR alone elicited moderate tumor growth delays, their efficacy was significantly enhanced when combined with GET of pDNA encoding CCL5, highlighting the synergy between these treatments. In CT26 tumors, combining GET with 25 μg of CCL5 and single-dose IR of 10 Gy achieved the longest tumor growth delay (15.0 ± 2.3 days) and up to 35 % CRs, demonstrating the effectiveness of the combined approach. Interestingly, tumor growth delays and CR rates were comparable between 25 and 50 μg of pDNA, demonstrating that increasing the pDNA dose does not result in significant increase of the therapeutic effect of CCL5. At 50 μg of pDNA, the effect of pDNA itself became more evident, as similar tumor growth delays were observed regardless of whether pDNA encoding CCL5 or non-coding pDNA Ctrl was used. Despite this, GET of pDNA encoding CCL5 consistently resulted in the highest immune memory development. Notably, in CT26 tumors GET of pDNA encoding CCL5 combined with IR 10 Gy led to 22.2 % CRs and only 20 % tumor regrowth in rechallenge experiments, indicating a robust and durable anti-tumor immune response.

Fractionated IR of 3 × 5 Gy further improved CT26 tumor growth delays when combined with GET of pDNA encoding CCL5 (up to 17.1 ± 1.7 days) and led to 47 % CRs. However, immune memory was less pronounced compared to single-dose IR, with higher tumor regrowth rates (67 %) after rechallenge. These encouraging results, could be associated with observed upregulation of inflammatory cytokines *Cxcl10*, *Ifn-γ* and *Il-12α* after combined therapies. Moreover, the success of combined therapies, especially with pDNA Ctrl and IR, could also be attributed to increased expression of DNA sensors such as cGAS, DAI, AIM-2, TREX1, and others [77–80]. These sensors, triggered by the presence of foreign DNA in the cytosol of cells, can disrupt tumor growth by upregulating the expression of inflammatory cytokines that synergistically contribute to activation of both innate and adaptive immune responses in combination with IR [81,82]. In 4T1 tumors combined treatment of GET of pDNA encoding CCL5 and single-dose IR of 10 Gy led to significantly longer tumor growth delay relative to both untreated control as well as equivalent treatment with control pDNA. However, CRs were limited. Although GET of pDNA encoding CCL5 combined with single-dose IR increased the expression of *Ccl5, Cxcl9*, *Cxcl10*, *Ifn-γ*, and *Il-12α*, this upregulation was insufficient to fully overcome the immunosuppressive barriers of the TME. This suggests that other immune cell populations, such as neutrophils, NK cells, MDSCs and Tregs, which were not evaluated in this study might play an important role in the immune response within treated tumors [83].

To preserve immune cells within tumors, partial tumor IR instead of whole-tumor IR is being extensively explored [84,85]. This approach requires precise treatment planning, often supported by image-guided techniques. For instance, Chen et al. [86] demonstrated that partial IR of 4T1-Luc tumors preserved CD4 + and CD8 + T lymphocytes and promoted DC activation, leading to increased survival in mice. These findings suggest that partial IR could improve outcomes when combined with immunotherapies. Moreover, partial tumor IR represents a potential strategy to maintain sufficient numbers of infiltrating immune cells while retaining the immunostimulatory benefits of radiotherapy; however, this approach was beyond the scope of the present study. Given the reduction in CD4 + and CD8 + T cells observed in our immunofluorescence analysis after combined treatments and considering that IR may kill immune cells, we tested a modified therapy involving double GET with 25 μg of pDNA and fractionated IR of 3×5 Gy. In this approach, a second GET was performed 24 h after the final IR dose to preserve and potentially enhance immune cell infiltration. Notably, double GET combined with fractionated IR led to increased expression of introduced CCL5, while the expression levels of other cytokines remained at basal levels. Although this strategy achieved overall longer tumor growth delays, it did not improve tumor cure rates or facilitate better immune memory formation compared to combined treatments of single GET and IR.

5. Conclusions

In summary, this study demonstrated the potential of combining GET of chemokine CCL5 with RT for solid tumors. CCL5-transfected tumor cells were shown to attract both macrophages in vitro and naïve splenocytes in DWCs in vivo. In immunogenic CT26 tumors, combined treatments significantly enhanced tumor growth delays and induced the formation of the immune memory. In non-immunogenic 4T1 tumors, combined therapy of GET of pDNA encoding CCL5 and IR significantly improved tumor growth delays but did not achieve CRs or immune memory, reflecting the challenges of overcoming an immunosuppressive TME. Future studies are warranted to explore partial tumor IR, optimize the timing of GET of pDNA encoding CCL5 in combination with IR, and evaluate co-expressing downstream effectors such as CXCL9, CXCL10 to potentially amplify the therapeutic effect.

CRediT authorship contribution statement

Tim Bozic: Writing – original draft, Visualization, Methodology, Investigation, Formal analysis, Data curation, Conceptualization. **Iva Santek:** Writing – review & editing, Investigation. **Ziva Pisljar:** Writing – review & editing, Investigation. **Simona Kranjc Brezar:** Writing – review & editing, Investigation. **Gregor Sersa:** Writing – review & editing, Supervision, Funding acquisition, Conceptualization. **Bostjan Markelc:** Writing – review & editing, Supervision, Methodology, Investigation, Conceptualization. **Maja Cemazar:** Writing – review & editing, Supervision, Funding acquisition, Conceptualization.

Funding

This research was funded by the Slovenian Research and Innovation Agency (ARIS) grants (no.: P3–0003 and Z3–50112) and ARIS postgraduate research funding program. The manuscript has been proofread via Rubriq, Academic Copy Editing and the Automated Language Editing Tool.

Declaration of Competing Interest

Authors declare that they have no competing interests.

Acknowledgments

We would like to thank Teja Valant for her technical assistance, as well as Srdjan Novaković, Simona Traven and Vita Šetrajčič Dragoš from the Department of Molecular Diagnostics (Institute of Oncology Ljubljana, Slovenia) for their support.

Appendix A. Supporting information

Supplementary data associated with this article can be found in the online version at doi:10.1016/j.biopha.2025.118887.

References

[1] N. Nagarsheth, M.S. Wicha, W. Zou, Chemokines in the cancer microenvironment and their relevance in cancer immunotherapy, Nat. Rev. Immunol. 17 (9) (2017) 559–572.
[2] M. Yi, T. Li, M. Niu, H. Zhang, Y. Wu, K. Wu, et al., Targeting cytokine and chemokine signaling pathways for cancer therapy, in: Signal Transduction and Targeted Therapy, 9, Springer Nature, 2024.
[3] D. Dangaj, M. Bruand, A.J. Grimm, C. Ronet, D. Barras, P.A. Duttagupta, et al., Cooperation between constitutive and inducible chemokines enables T cell engraftment and immune attack in solid tumors, Cancer Cell 35 (6) (2019) 885–900, e10.
[4] J.W. Griffith, C.L. Sokol, A.D. Luster, Chemokines and chemokine receptors: positioning cells for host defense and immunity, Annu Rev. Immunol. 32 (1) (2014) 659–702.
[5] T. Wieder, T. Eigentler, E. Brenner, M. Röcken, Immune checkpoint blockade therapy, J. Allergy Clin. Immunol. 142 (5) (2018) 1403–1414. Nov 1.
[6] L. Galluzzi, T.A. Chan, G. Kroemer, J.D. Wolchok, A. López-Soto, The hallmarks of successful anticancer immunotherapy, Sci. Transl. Med 10 (459) (2018) 1–15.
[7] N. Kanagawa, M. Niwa, Y. Hatanaka, Y. Tani, S. Nakagawa, T. Fujita, et al., CC-chemokine ligand 17 gene therapy induces tumor regression through augmentation of tumor-infiltrating immune cells in a murine model of preexisting CT26 colon carcinoma, Int J. Cancer 121 (9) (2007) 2013–2022.
[8] O. Chan, J.D. Burke, D.F. Gao, E.N. Fish, The chemokine CCL5 regulates glucose uptake and AMP kinase signaling in activated T cells to facilitate chemotaxis, J. Biol. Chem. 287 (35) (2012) 29406–29416.
[9] G. An, F. Wu, S. Huang, L. Feng, J. Bai, S. Gu, et al., Effects of CCL5 on the biological behavior of breast cancer and the mechanisms of its interaction with tumor-associated macrophages, Oncol. Rep. 42 (6) (2019) 2499–2511.
[10] A. González-Martín, L. Gómez, J. Lustgarten, E. Mira, S.Maximal Mañes, T cell-mediated antitumor responses rely upon CCR5 expression in both CD4+ and CD8+ T cells, Cancer Res 71 (16) (2011) 5455–5466.
[11] J.P. Böttcher, E. Bonavita, P. Chakravarty, H. Blees, M. Cabeza-Cabrerizo, S. Sammicheli, et al., NK cells stimulate recruitment of cDC1 into the tumor microenvironment promoting cancer immune control, Cell 172 (5) (2018) 1022–1037, e14.
[12] O. Melaiu, M. Chierici, V. Lucarini, G. Jurman, L.A. Conti, R. De Vito, et al., Cellular and gene signatures of tumor-infiltrating dendritic cells and natural-killer cells predict prognosis of neuroblastoma, Nat. Commun. [Internet] 11 (1) (2020) 1–15, https://doi.org/10.1038/s41467-020-19781-y.
[13] J.M. Araujo, A.C. Gomez, A. Aguilar, R. Salgado, J.M. Balko, L. Bravo, et al., Effect of CCL5 expression in the recruitment of immune cells in triple negative breast cancer, Sci. Rep. [Internet] 8 (1) (2018) 1–9, https://doi.org/10.1038/s41598-018-23099-7.
[14] M.K. Kranjc, M. Novak, R.G. Pestell, T.T. Lah, Cytokine CCL5 and receptor CCR5 axis in glioblastoma multiforme, Radio. Oncol. 53 (4) (2019) 397–406.
[15] S. Trellakis, K. Bruderek, C.A. Dumitru, H. Gholaman, X. Gu, A. Bankfalvi, et al., Polymorphonuclear granulocytes in human head and neck cancer: enhanced inflammatory activity, modulation by cancer cells and expansion in advanced disease, Int J. Cancer 129 (9) (2011) 2183–2193.
[16] N.M. Kaskas, T. Moore-Medlin, G.B. McClure, O. Ekshyyan, J.A. Vanchiere, C.A. O. Nathan, Serum biomarkers in head and neck squamous cell cancer, JAMA Otolaryngol. Head. Neck Surg. 140 (1) (2014) 5–11.
[17] M. Sadeghi, I. Lahdou, H. Oweira, V. Daniel, P. Terness, J. Schmidt, et al., Serum levels of chemokines CCL4 and CCL5 in cirrhotic patients indicate the presence of hepatocellular carcinoma, Br. J. Cancer [Internet] 113 (5) (2015) 756–762, https://doi.org/10.1038/bjc.2015.227.
[18] E.J. Duell, D.P. Casella, R.D. Burk, K.T. Kelsey, E.A. Holly, Inflammation, genetic polymorphisms in proinflammatory genes TNF-A, RANTES, and CCR5, and risk of pancreatic adenocarcinoma, Cancer Epidemiol. Biomark. Prev. 15 (4) (2006) 726–731.
[19] G.G. Vaday, D.M. Peehl, P.A. Kadam, D.M. Lawrence, Expression of CCL5 (RANTES) and CCR5 in prostate cancer, Prostate 66 (2) (2006) 124–134.
[20] R. Huang, S. Wang, N. Wang, Y. Zheng, J. Zhou, B. Yang, et al., CCL5 derived from tumor-associated macrophages promotes prostate cancer stem cells and metastasis via activating β-catenin/STAT3 signaling, Cell Death Dis. 11 (4) (2020). Apr 1.
[21] J. Wang, Y. Wang, F. Kong, R. Han, W. Song, D. Chen, et al., Identification of a six-gene prognostic signature for oral squamous cell carcinoma, J. Cell Physiol. 235 (3) (2020) 3056–3068.
[22] Y. Fujimoto, N. Inoue, K. Morimoto, T. Watanabe, S. Hirota, M. Imamura, et al., Significant association between high serum CCL5 levels and better disease-free survival of patients with early breast cancer, Cancer Sci. 111 (1) (2020) 209–218.
[23] N. Lapteva, X.F. Huang, CCL5 as an adjuvant for cancer immunotherapy, Expert Opin. Biol. Ther. 10 (5) (2010) 725–733.
[24] D. Peng, I. Kryczek, N. Nagarsheth, L. Zhao, S. Wei, W. Wang, et al., Epigenetic silencing of TH1-type chemokines shapes tumour immunity and immunotherapy (Available from:), Nat. [Internet] 527 (7577) (2015) 249–253, https://doi.org/10.1038/nature15520.
[25] H. Aboulkheyr Es, B. Bigdeli, S. Zhand, A.R. Aref, J.P. Thiery, M.E. Warkiani, Mesenchymal stem cells induce PD-L1 expression through the secretion of CCL5 in breast cancer cells, J. Cell Physiol. 236 (5) (2021) 3918–3928. May 1.
[26] K. Ganesh, Z.K. Stadler, A. Cercek, R.B. Mendelsohn, J. Shia, N.H. Segal, et al., Immunotherapy in colorectal cancer: rationale, challenges and potential (Available from:), Nat. Rev. Gastroenterol. Hepatol. [Internet] 16 (6) (2019) 361–375, https://doi.org/10.1038/s41575-019-0126-x.
[27] Z. Zhang, X. Liu, D. Chen, J. Yu, Radiotherapy combined with immunotherapy: the dawn of cancer treatment, in: Signal Transduction and Targeted Therapy, 7, Springer Nature, 2022.
[28] K.A. Pilones, C. Vanpouille-Box, S. Demaria, Combination of radiotherapy and immune checkpoint inhibitors, in: Seminars in Radiation Oncology, 25, W.B. Saunders, 2015, pp. 28–33.
[29] J. Constanzo, J. Faget, C. Ursino, C. Badie, J.P. Pouget, Radiation-induced immunity and toxicities: the versatility of the cGAS-STING pathway, in: Frontiers in Immunology, 12, Frontiers Media S.A., 2021.
[30] S. Zhu, Y. Wang, J. Tang, M. Cao, Radiotherapy induced immunogenic cell death by remodeling tumor immune microenvironment, Front Immunol. 13 (December) (2022) 1–20.
[31] T. Bozic, G. Sersa, S. Kranjc Brezar, M. Cemazar, B. Markelc, Gene electrotransfer of proinflammatory chemokines CCL5 and CCL17 as a novel approach of modifying cytokine expression profile in the tumor microenvironment, Bioelectrochemistry [Internet] 140 (2021) 107795, https://doi.org/10.1016/j.bioelechem.2021.107795.

[32] L. Galluzzi, T.A. Chan, G. Kroemer, J.D. Wolchok, A. López-Soto, The hallmarks of successful anticancer immunotherapy, Sci. Transl. Med 10 (459) (2018) 1–15.
[33] N. Percie Du Sert, V. Hurst, A. Ahluwalia, S. Alam, M.T. Avey, M. Baker, et al., The ARRIVE guidelines 2.0: updated guidelines for reporting animal research, BMC Vet. Res [Internet] 16 (1) (2020) 1–7. Available from: ⟨https://bmcvetres.biomedcentral.com/articles/10.1186/s12917-020-02451-y⟩.
[34] A.J. Smith, R.E. Clutton, E. Lilley, K.E.A. Hansen, T. Brattelid, PREPARE: guidelines for planning animal research and testing, Lab Anim. [Internet] 52 (2) (2018) 135–141. Available from: ⟨https://pubmed.ncbi.nlm.nih.gov/28771074/⟩.
[35] S.I. De Vleeschauwer, M. van de Ven, A. Oudin, K. Debusschere, K. Connor, A. T. Byrne, et al., OBSERVE: guidelines for the refinement of rodent cancer models, Nat. Protoc. 19 (9) (2024) 2571–2596.
[36] T. Bozic, B. Markelc, Imaging of extravasation of splenocytes in the dorsal skinfold window chamber, in: M. Čemažar, T. Jesenko, Tratar U. Lampreht (Eds.), Mouse Models of Cancer: Methods and Protocols [Internet], Springer US, New York, NY, 2024, pp. 137–155, https://doi.org/10.1007/978-1-0716-3714-2_13.
[37] D.J. Langford, A.L. Bailey, M.L. Chanda, S.E. Clarke, T.E. Drummond, S. Echols, et al., Coding of facial expressions of pain in the laboratory mouse, Nat. Methods [Internet] 7 (6) (2010) 447–449, https://doi.org/10.1038/nmeth.1455.
[38] L.M. Mir, J. Gehl, G. Sersa, C.G. Collins, J.R. Garbay, V. Billard, et al., Standard operating procedures of the electrochemotherapy: instructions for the use of bleomycin or cisplatin administered either systemically or locally and electric pulses delivered by the CliniporatorTM by means of invasive or non-invasive electrodes, in: European Journal of Cancer, 4, Supplement, 2006, pp. 14–25.
[39] J. Gehl, G. Sersa, L.W. Matthiessen, T. Muir, D. Soden, A. Occhini, et al., Updated standard operating procedures for electrochemotherapy of cutaneous tumours and skin metastases, Acta Oncol. (Madr.) [Internet] 57 (7) (2018) 874–882, https://doi.org/10.1080/0284186X.2018.1454602.
[40] V. Todorovic, U. Kamensek, G. Sersa, M. Cemazar, Changing electrode orientation, but not pulse polarity, increases the efficacy of gene electrotransfer to tumors in vivo, Bioelectrochemistry 100 (2014 Dec 1) 119–127.
[41] C.M. van Leeuwen, A.L. Oei, J. Crezee, A. Bel, N.A.P. Franken, L.J.A. Stalpers, et al., The alfa and beta of tumours: a review of parameters of the linear-quadratic model, derived from clinical radiotherapy studies, Radiat. Oncol. 13 (1) (2018) 1–11.
[42] Q. Li, W. Dai, J. Liu, Y.X. Li, Y.Y. Li, DRAP: a toolbox for drug response analysis and visualization tailored for preclinical drug testing on patient-derived xenograft models, J. Transl. Med [Internet] 17 (1) (2019) 13–16, https://doi.org/10.1186/s12967-019-1785-7.
[43] H. Miao, J.A. Hollenbaugh, M.S. Zand, J. Holden-Wiltse, T.R. Mosmann, A. S. Perelson, et al., Quantifying the early immune response and adaptive immune response kinetics in mice infected with influenza A virus, J. Virol. 84 (13) (2010) 6687–6698.
[44] Z. Chen, F. Han, Y. Du, H. Shi, W. Zhou, Hypoxic microenvironment in cancer: molecular mechanisms and therapeutic interventions, in: Signal Transduction and Targeted Therapy, 8, Springer Nature, 2023.
[45] N. Kumari, B.S. Dwarakanath, A. Das, A.N. Bhatt, Role of interleukin-6 in cancer progression and therapeutic resistance, Tumor Biol. [Internet] 37 (9) (2016) 11553–11572, https://doi.org/10.1007/s13277-016-5098-7.
[46] D. Peng, I. Kryczek, N. Nagarsheth, L. Zhao, S. Wei, W. Wang, et al., Epigenetic silencing of TH1-type chemokines shapes tumour immunity and immunotherapy, Nature 527 (7577) (2015) 249–253.
[47] A.D. Garg, A.M. Dudek-Peric, E. Romano, P. Agostinis, Immunogenic cell death, Int. J. Dev. Biol. 59 (1–3) (2015) 131–140.
[48] S. Guo, Y. Yao, Y. Tang, Z. Xin, D. Wu, C. Ni, et al., Radiation-induced tumor immune microenvironments and potential targets for combination therapy, in: Signal Transduction and Targeted Therapy, 8, Springer Nature, 2023.
[49] A.M. Monjazeb, K.A. Schalper, F. Villarroel-Espindola, A. Nguyen, S.L. Shiao, K. Young, Effects of radiation on the tumor microenvironment, Semin Radiat. Oncol. 30 (2) (2020 Apr 1) 145–157.
[50] T. Yamazaki, K.H. Young, Effects of radiation on tumor vasculature, Mol. Carcinog. 61 (2) (2022 Feb 1) 165–172.
[51] K.M. Arnold, N.J. Flynn, A. Raben, L. Romak, Y. Yu, A.P. Dicker, et al., The impact of radiation on the tumor microenvironment: effect of dose and fractionation schedules, Cancer Growth Metastas.. 11 (2018 Jan 1).
[52] C. Rosazza, S.H. Meglic, A. Zumbusch, M.P. Rols, D. Miklavcic, Gene electrotransfer: a mechanistic perspective, Curr. Gene Ther. [Internet] 16 (2016) 98–129. Available from: ⟨http://clinicaltrials.gov⟩.
[53] M. Bosnjak, B.C. Lorente, Z. Pogacar, V. Makovsek, M. Cemazar, Different incubation times of cells after gene electrotransfer in fetal bovine serum affect cell viability, but not transfection efficiency, J. Membr. Biol. 247 (5) (2014) 421–428.
[54] E. Sieni, M. Dettin, M. De Robertis, B. Bazzolo, M.T. Conconi, A. Zamuner, et al., The efficiency of gene electrotransfer in breast-cancer cell lines cultured on a novel collagen-free 3D scaffold, Cancers (Basel) 12 (4) (2020).
[55] M. De Robertis, L. Pasquet, L. Loiacono, E. Bellard, L. Messina, S. Vaccaro, et al., In vivo evaluation of a new recombinant hyaluronidase to improve gene electrotransfer protocols for dna-based drug delivery against cancer, Cancers (Basel) 10 (11) (2018).
[56] V. Mlakar, V. Todorovic, M. Cemazar, D. Glavac, G. Sersa, Electric pulses used in electrochemotherapy and electrogene therapy do not significantly change the expression profile of genes involved in the development of cancer in malignant melanoma cells, BMC Cancer 9 (2009) 299.
[57] A. Masotti, G. Mossa, C. Cametti, G. Ortaggi, A. Bianco, N.Del Grosso, et al., Comparison of different commercially available cationic liposome-DNA lipoplexes: Parameters influencing toxicity and transfection efficiency, Colloids Surf. B Biointerfaces 68 (2) (2009) 136–144.
[58] L.D. Bennett, J.M. Fox, N. Signoret, Mechanisms regulating chemokine receptor activity, Immunology 134 (2011) 246–256.
[59] B. Schrörs, S. Boegel, C. Albrecht, T. Bukur, V. Bukur, C. Holtsträter, et al., Multi-omics characterization of the 4T1 murine mammary gland tumor model, Front Oncol. 10 (2020 Jul 23).
[60] S.I.S. Mosely, J.E. Prime, R.C.A. Sainson, J.O. Koopmann, D.Y.Q. Wang, D. M. Greenawalt, et al., Rational selection of syngeneic preclinical tumor models for immunotherapeutic drug discovery, Cancer Immunol. Res 5 (1) (2017) 29–41.
[61] T. Fu, L.J. Dai, S.Y. Wu, Y. Xiao, D. Ma, Y.Z. Jiang, et al., Spatial architecture of the immune microenvironment orchestrates tumor immunity and therapeutic response, in: Journal of Hematology and Oncology, 14, BioMed Central Ltd, 2021.
[62] M. Binnewies, E.W. Roberts, K. Kersten, V. Chan, D.F. Fearon, M. Merad, et al., Understanding the tumor immune microenvironment (TIME) for effective therapy, Nat. Med 24 (5) (2018 May 1) 541–550.
[63] B. Markelc, E. Bellard, G. Sersa, S. Pelofy, J. Teissie, A. Coer, et al., In vivo molecular imaging and histological analysis of changes induced by electric pulses used for plasmid dna electrotransfer to the skin: a study in a dorsal window chamber in mice, J. Membr. Biol. 245 (9) (2012) 545–554.
[64] M. De Robertis, T. Bozic, I. Santek, F. Marzano, B. Markelc, D.A. Silvestris, et al., Transcriptomic analysis of the immune response to in vivo gene electrotransfer in colorectal cancer, Mol. Ther. Nucleic Acids 36 (1) (2025 Mar 11).
[65] S. Guo, Y. Yao, Y. Tang, Z. Xin, D. Wu, C. Ni, et al., Radiation-induced tumor immune microenvironments and potential targets for combination therapy, in: Signal Transduction and Targeted Therapy, 8, Springer Nature, 2023.
[66] S. Demaria, C. Guha, J. Schoenfeld, Z. Morris, A. Monjazeb, A. Sikora, et al., Radiation dose and fraction in immunotherapy: one-size regimen does not fit all settings, so how does one choose?, in: Journal for ImmunoTherapy of Cancer, 9 BMJ Publishing Group, 2021.
[67] I.G. House, P. Savas, J. Lai, A.X.Y. Chen, A.J. Oliver, Z.L. Teo, et al., Macrophage-derived CXCL9 and CXCL10 are required for antitumor immune responses following immune checkpoint blockade, Clin. Cancer Res. 26 (2) (2020) 487–504.
[68] E.C. Keeley, B. Mehrad, R.M. Strieter, Chemokines as mediators of tumor angiogenesis and neovascularization, Exp. Cell Res 317 (5) (2011) 685–690.
[69] A. Kano, Tumor cell secretion of soluble factor(s) for specific immunosuppression, Sci. Rep. 5 (2015) 1–8.
[70] M. Cemazar, T. Jarm, G. Sersa, Cancer electrogene therapy with interleukin-12, Curr. Gene Ther. 10 (4) (2010) 300–311.
[71] K.G. Nguyen, M.R. Vrabel, S.M. Mantooth, J.J. Hopkins, E.S. Wagner, T. A. Gabaldon, et al., Localized interleukin-12 for cancer immunotherapy, Front Immunol. 11 (October) (2020) 1–36.
[72] U. Lampreht Tratar, L. Loiacono, M. Cemazar, U. Kamensek, V.M. Fazio, G. Sersa, et al., Gene Electrotransfer of plasmid-encoding IL-12 recruits the M1 macrophages and antigen-presenting cells inducing the eradication of aggressive B16F10 murine melanoma, Mediat. Inflamm. 2017 (2017).
[73] E.H. Cheteh, V. Sarne, S. Ceder, J. Bianchi, M. Augsten, H. Rundqvist, et al., Interleukin-6 derived from cancer-associated fibroblasts attenuates the p53 response to doxorubicin in prostate cancer cells, Cell Death Discov. [Internet] 6 (1) (2020), https://doi.org/10.1038/s41420-020-0272-5.
[74] C.M. Lloyd, R.J. Snelgrove, Type 2 immunity: Expanding our view [Internet], Sci. Immunol. 3 (2018). Available from: ⟨http://immunology.sciencemag.org/⟩.
[75] K. De Jaeger, F.M. Merlo, M.C. Kavanagh, A.W. Fyles, D. Hedley, R.P. Hill, Heterogeneity of tumor oxygenation: relationship to tumor necrosis, tumor size, and metastasis, Int. J. Radiat. Oncol. *Biol. *Phys. [Internet] 42 (4) (1998) 717–721. ⟨https://www.sciencedirect.com/science/article/pii/S036030169800323X⟩.
[76] A. Meirovitz, M. Gross, S. Cohen, A. Popovtzer, V. Barak, Effect of irradiation on cytokine production in cancer patients, Int. J. Biol. Markers 37 (4) (2022 Dec 1) 360–367.
[77] S. Luecke, A. Holleufer, M.H. Christensen, K.L. Jønsson, G.A. Boni, L.K. Sørensen, et al., cGAS is activated by DNA in a length-dependent manner, EMBO Rep. 18 (10) (2017) 1707–1715.
[78] K. Znidar, M. Bosnjak, M. Cemazar, L.C. Heller, Cytosolic DNA sensor upregulation accompanies DNA electrotransfer in B16.F10 melanoma cells, Mol. Ther. Nucleic Acids 5 (6) (2016) e322.
[79] C. Vanpouille-Box, A. Alard, M.J. Aryankalayil, Y. Sarfraz, J.M. Diamond, R. J. Schneider, et al., DNA exonuclease Trex1 regulates radiotherapy-induced tumour immunogenicity, Nat. Commun. 8 (2017) 15618.
[80] T. Jesenko, M. Bosnjak, B. Markelc, G. Sersa, K. Znidar, L. Heller, et al., Radiation induced upregulation of dna sensing pathways is cell-type dependent and can mediate the off-target effects, Cancers (Basel) 12 (11) (2020 Nov 1) 1–23.
[81] N. Semenova, M. Bosnjak, B. Markelc, K. Znidar, M. Cemazar, L. Heller, Multiple cytosolic DNA sensors bind plasmid DNA after transfection, Nucleic Acids Res 47 (19) (2019) 10235–10246.
[82] T. Jesenko, M. Bosnjak, B. Markelc, G. Sersa, K. Znidar, L. Heller, et al., Radiation induced upregulation of DNA sensing pathways is cell-type dependent and can mediate the off-target effects, Cancers (Basel) 12 (11) (2020) 1–23.
[83] C. Zalfa, S. Paust, Natural Killer Cell Interactions With Myeloid Derived Suppressor Cells in the Tumor Microenvironment and Implications for Cancer Immunotherapy, in: Frontiers in Immunology, 12, Frontiers Media S.A., 2021.
[84] S. Tubin, H.H. Popper, L. Brcic, Novel stereotactic body radiation therapy (SBRT)-based partial tumor irradiation targeting hypoxic segment of bulky tumors (SBRT-

PATHY): improvement of the radiotherapy outcome by exploiting the bystander and abscopal effects, Radiat. Oncol. 14 (1) (2019) 1–11.
[85] Z. Pisljar, B. Markelc, S.K. Brezar, T. Bozic, G. Sersa, M. Cemazar, et al., Partial versus whole tumor-volume irradiation in combination with immunotherapy: comparable outcomes in immunosuppressed mouse models of oral squamous cell carcinoma, Biomed. Pharmacother. 187 (2025 Jun 1).
[86] H. Chen, Y. Li, Q. Shen, G. Guo, Z. Wang, H. Pan, et al., Reduced irradiation exposure areas enhanced anti-tumor effect by inducing DNA damage and preserving lymphocytes, Mol. Med. 30 (1) (2024 Dec 1).